Title

Innovations in Instrumentation for Positron Emission Tomography

Journal

Seminars in Nuclear Medicine, 48(4)

ISSN

0001-2998

Authors

Berg, Eric

Cherry, Simon R

Publication Date

2018-07-01

DOI

10.1053/j.semnuclmed.2018.02.006

Peer reviewed

HHS Public Access

Author manuscript

Semin Nucl Med. Author manuscript; available in PMC 2019 July 01.

Published in final edited form as:

Semin Nucl Med. 2018 July ; 48(4): 311–331. doi:10.1053/j.semnuclmed.2018.02.006.

Innovations in instrumentation for positron emission tomography

Eric Berg, Ph.D.[1] and **Simon R. Cherry, Ph.D.**[1,2]

[1]Department of Biomedical Engineering

[2]Department of Radiology University of California, Davis

Abstract

Positron emission tomography (PET) scanners are sophisticated and highly sensitive biomedical imaging devices that can produce highly quantitative images showing the three-dimensional distribution of radiotracers inside the body. PET scanners are commonly integrated with x-ray computed tomography (CT) or magnetic resonance imaging (MRI) scanners in hybrid devices that can provide both molecular imaging (PET) and anatomical imaging (CT or MRI). Despite decades of development, significant opportunities still exist to make major improvements in the performance of PET systems for a variety of clinical and research tasks. These opportunities stem from new ideas and concepts, as well as a range of enabling technologies and methodologies. In this paper, we review current state of the art in PET instrumentation, detectors and systems, describe the major limitations in PET as currently practiced, and offer our own personal insights into some of the recent and emerging technological innovations that we believe will impact the field. Our focus is on the technical aspects of PET imaging, specifically detectors and system design, and the opportunity and necessity to move closer to PET systems for diagnostic patient use and *in vivo* biomedical research that truly approach the physical performance limits while remaining mindful of imaging time, radiation dose and cost. However, other key endeavors which are not covered here, including innovations in reconstruction and modeling methodology, radiotracer development, and expanding the range of clinical and research applications, also will play an equally important, if not more important, role in defining the future of the field.

1. Introduction

Positron emission tomography (PET) is a nuclear medicine imaging technique based on the injection of radiotracers labeled with a positron-emitting radionuclide [1, 2]. The power of the technique lies in the wide range of available radiotracers [3] that produce image contrast directly related to underlying physiology, metabolic pathways or molecular targets. Using today's advanced PET scanners, radiotracers can readily be detected at trace mass levels

Corresponding Author: Simon R. Cherry, Ph.D., Department of Biomedical Engineering, University of California, Davis, 451 Health Sciences Drive, Davis, CA 95616, ***Phone:*** (530) 754-9419, srcherry@ucdavis.edu.

(nanomolar concentrations or less), and using a dynamic sequence of images and the principles of tracer kinetic modeling, parameters related to the transport, metabolism and or binding of the tracer can be quantitatively derived [4]. Positron-emitting radionuclides also can be used to label drugs, cellular therapies or particles designed for nanomedicine, to conduct pharmacokinetic studies. Despite the potential for broad use of PET imaging in many disease states, its application has been quite constrained by a combination of factors, some technical, which are addressed in this review, and some which relate to a complex interplay of practice, regulatory, economic and perceptual issues.

Positron-emitting radionuclides were first imaged in the 1950s [5, 6] and the predecessors of today's clinical positron emission tomography (PET) systems were developed in the 1970s [1, 7, 8]. PET is now firmly established as one of the major biomedical imaging modalities, with applications spanning basic human research, clinical research, clinical trials and routine clinical diagnostic imaging. PET also has become established as a translational imaging modality, with the development and adoption of preclinical scanners [9], for imaging animals small (mice, rats) and large (dogs, nonhuman primates). We also have witnessed the successful integration of PET first with x-ray computed tomography (CT) [10], and subsequently with magnetic resonance imaging (MRI) [11], to create powerful hybrid imaging systems that can interrogate structure and function in the same imaging examination [12]. After many decades of technological development, and some sense of stability and maturity in current commercial products, it is tempting to conclude that our work is mostly done. However, several potentially disruptive technologies, methodologies and concepts loom large in the landscape today, offering new directions and possibilities that could dramatically change the way and the degree to which PET is used in biomedical research and healthcare. These include scanners with much higher geometric coverage of the body, very sensitive and compact silicon photomultiplier light sensors, fast detectors for time-of-flight PET using traditional scintillation light or other prompt emissions, and fast electronics combined with computational methods to better estimate the location, time and energy of an interaction in the detector. In this review, we describe these and other innovations, which ultimately offer the prospect of realizing the full potential of PET and the tracer kinetic principles on which it is based.

2. Current Status, Limitations and Opportunities

First, a little background will be useful to follow the arguments made throughout this article. The signal that is used to form a PET image comes from the coincidence detection of the two back-to-back 511 keV annihilation photons emitted when a positron-emitting radionuclide (typically attached to a radiotracer) decays inside the body [13]. On the order of 10^7 to 10^8 decay events are collected by detectors that surround the patient and used to reconstruct a PET image that reflects the distribution of the radionuclide (and thus the radiotracer it is attached to) in the body. Quite often, one or even both the annihilation photons will scatter in the patient and change direction, in the process losing some of their energy. These are called *scattered events*. It also is possible for two photons from unrelated radionuclide decays to strike the detectors at almost the same time, thus appearing to produce a valid coincidence event. These are called *random events*. The number of both scattered and random events should be minimized to obtain the highest quality images, as

the coincidence detection of these events does not represent the back-to-back nature of annihilation photons upon which PET is based. Lastly, the two annihilation photons will reach the detectors at slightly different times depending on the distance each annihilation photon has to travel from the site of production to the detectors. The ability of a PET scanner to measure this time difference is referred to as *time-of-flight PET*. The use of time-of-flight information in the image reconstruction helps localize the event and improves image quality through suppressing the contribution of random and scatter events [14]. Theoretically, it is possible to use time-of-flight information to directly localize the annihilation site along the line connecting a detector pair without the need for a reconstruction algorithm, however, as light travels at about 30 cm per nanosecond, the difference in arrival time changes by only ~67 picoseconds per 1 cm difference in location. PET detectors do not currently have the necessary timing resolution needed for direct reconstruction with adequate spatial resolution (5 mm or better). Therefore, all PET scans still need a reconstruction algorithm to take the line segments defined by each detected event and reconstruct these into a quantitative image where the image intensity reflects the radiotracer activity per unit tissue volume (kBq/cc). Modern reconstruction methods are reviewed in [15].

The basic detection unit used in almost all PET scanners is a *scintillation detector*, consisting of a dense scintillator crystal coupled to a sensitive light detector (*photodetector*). An incoming 511 keV annihilation photon can interact in the scintillation crystal, depositing some or all of its energy and producing a short flash of visible light over a time period governed by the decay time of the scintillator. This decay time is generally in the range of tens to a few hundreds of nanoseconds, and during this period a few thousand visible light photons are typically produced depending on the scintillator composition and the amount of energy deposited. Since the scintillator light output is approximately proportional to the deposited energy, measuring the amount of light produced in the scintillator can be used to reject a large fraction of scattered annihilation photons. The light is converted by the photodetector into electrons and amplified, leading to an electronic output pulse that signals the detection of an event. The detection of two events in the scanner at approximately the same time (e.g. within +/− 2 ns for clinical imaging) signifies the likely detection of both annihilation photons emitted following a decay from the positron-emitting source somewhere along the path between the coincident detectors, and represents a valid coincidence event.

If one looks back over several decades of development, the performance of PET scanners can be seen to have improved dramatically [1, 2]. From the earliest single ring cameras, to multi-ring cameras and then fully 3D systems, sensitivity has improved by more than two orders of magnitude, and combined with brighter and faster scintillators, and more sensitive photodetectors, this also has led to significant improvements in spatial resolution, energy resolution (controlling scatter) and timing resolution (reducing the impact of random events and enabling time-of-flight PET to become routinely implemented). Parallel advances in electronics (enabling higher counting rate capabilities and improved system stability) and computing power (leading to routine use of iterative image reconstruction methods) have also played important roles in producing clinical PET scans that are clearly superior, and acquired in considerably shorter times, than those from three decades ago. Commercial clinical scanners have converged on a fairly consistent design, with scintillation crystals

typically with dimensions of 3–4 mm on a side by 15–25 mm deep, coupled to sensitive photodetectors (most commonly, silicon photomultipliers (SiPMs)) and arranged in 80–90 cm diameter rings around the subject, while covering an axial extent along the body of 15–30 cm. Most scanners have time-of-flight capability and are integrated with CT (most commonly), or with MRI, to form powerful hybrid diagnostic instruments. Most modern systems achieve a reconstructed spatial resolution of 3–5 mm in each direction, an overall sensitivity (based on a standard test protocol defined by the National Electrical Manufacturers Association [16]) of ~10–20 cps/kBq, and an energy resolution of 10–12%. For time-of-flight performance, which has been the most intense area of recent focus and improvement, some clinical systems now achieve 400 psecs or better [17, 18], and current developments suggest that systems with 250 ps timing will be available soon. In the preclinical arena, there has been more of a stress on spatial resolution, with compact systems designed for rodent imaging producing images with a spatial resolution in the 1–2 mm range [9].

Despite the impressive gains in the performance of PET scanners, there of course have been similarly stunning advances in most of the other imaging modalities as well. Thus, the same criticisms that were levelled at PET many decades ago, namely the relatively poor photon statistics that lead to low signal-to-noise ratio (SNR) images, and the limited spatial resolution, are the same limitations identified today. Therefore, the focus of this article is to address these limitations and ask the question as to whether today's scanners approach the fundamental limits imposed by the physics of signal production, detection and processing, or whether we can make a case that there is still much to be done and room for further significant gains. Another key focus are improvements that benefit patients, that may not necessarily be linked to performance improvements. For example, the ability to acquire diagnostic quality scans faster, at lower radiation dose or at lower cost. Radiation dose burden and cost, in particular, are factors widely perceived to limit the broader application of PET, both in clinical care and research studies.

Limitation 1: Low image SNR

The SNR is a critical measure of image quality, and in PET imaging, to first order, is determined by the number of detected events (pairs of annihilation photons detected in time coincidence), n:

$$SNR \propto \sqrt{n} \quad \text{(Eq. 1)}$$

Low SNR negatively impacts the ability to detect small lesions, quantification of radiotracer activity in a structure, and is a common feature in dynamic imaging because of the difficulty of collecting sufficient number of events in the short imaging times typically needed to capture the early rapid changes in distribution that occur in the first few minutes after radiotracer injection. Low SNR is arguably the biggest technical limitation in PET imaging today, as it also plays a central role in each of the other limitations identified below.

The number of events acquired in a PET scan is given approximately by:

$$n \approx kAG\varepsilon^2 T \quad \text{(Eq. 2)}$$

where A is the amount of activity in the scanner's field of view (assumed to be uniformly distributed), G is the average geometric coverage of the scanner, ε is the efficiency of the detector for converting an incident 511 keV photon into a detected event (and is squared because both photons must be detected for a valid event), T is the acquisition time and k accounts for patient-specific factors such as attenuation and scatter of the photons in the body. This formulation assumes that the scan time t is sufficiently short compared to the half-life of the radionuclide being imaged so that radioactive decay can be ignored, and that loss of events from detector or system dead time is negligible.

The SNR also can be improved by improving the time-of-flight resolution of a PET scanner. The relationship between SNR and the timing resolution Δt, is given by [19, 20]

$$SNR \propto \sqrt{D/\Delta t} \quad \text{(Eq. 3)}$$

where D is the diameter of the object being imaged. Combining Eqs. 1–3, we can express the expected SNR in a reconstructed PET image as:

$$SNR \approx \sqrt{\frac{k' AG\varepsilon^2 T}{\Delta t}} \quad \text{(Eq. 4)}$$

where k' not only includes the factor k in Eq. 2, but also incorporates the diameter of the subject, D, factors related to the reconstruction algorithm as well as uncertainties that may be introduced by other corrections applied to the collected data. As Eq. 4 shows, to increase SNR, the choices are to increase A (but this increases radiation dose), lengthen the scan time T (also undesirable due to patient comfort and clinical throughput), improve the efficiency with which the PET scanner detects the emitted radiation by increasing G and/or ε, or improve the timing resolution Δt. PET scans already use activities which lead to a radiation burden of 5–8 mSv for a typical diagnostic scan, and imaging times of 10–20 minutes. Thus, the key question is to determine to what extent improvements in G, ε and/or Δt are possible to address current SNR limitations in PET.

Limitation 2: Low spatial resolution

The fundamental limits of spatial resolution achievable in PET are ultimately determined by the physics of the positron decay and annihilation. Firstly, the positron, once emitted from a decaying atom, travels a short distance before it annihilates and produces the two 511 keV photons that ultimately are detected to form an event. This distance, known as the *positron range*, depends on the energy of the emitted positrons. For fluorine-18 (^{18}F), which emits relatively low-energy positrons, this distance is typically less than 0.5 mm. For most other radionuclides the range is higher and can reach values as high as several mm. Secondly,

because the positron, and the electron with which it annihilates, are not completely at rest when the annihilation occurs, the two 511 keV photons are not emitted exactly 180° apart, an effect called *non-colinearity*. Rather, there is a distribution of about 0.2° around the 180° mean value. This leads to increasing location errors as the distance between the detectors increases and is therefore a major limiting factor for a whole-body PET scanner which requires a large bore to accommodate the patient. Assuming a detector ring diameter of 80 cm, the blurring from this effect is ~1.8 mm. In a small diameter preclinical scanner for rodent imaging, with say a 12 cm diameter detector ring, the blurring from non-colinearity is only around 0.26 mm. From these considerations, one can estimate that the best spatial resolution achievable when imaging a ^{18}F-labeled radiotracer with PET is approximately 2 mm in a human whole-body scanner, and around 0.4 mm in a small-diameter rodent imaging system [21].

Current scanners typically are not achieving these levels of spatial resolution in reconstructed images. Partly this is because of the physical size of the detector elements, which further limits the spatial resolution and sampling. But mostly, the practical limitation comes once again from the limited number of detected events as described in the previous section. In a typical scanning scenario there are just not sufficient number of events per resolution element to reconstruct images at the limiting spatial resolution at an acceptable SNR. Thus solving the SNR limitation is also key to solving the spatial resolution limitation.

Limitation 3: Long scan times, relatively high radiation burden

From the patient's perspective, two common areas of concern relate to the radiation dose received from a PET scan, and the discomfort of lying as still as possible for 10–20 minutes, knowing that even small movements during this time can blur the images and reduce the accuracy of diagnostic interpretation. However, reducing either of these factors, as shown in Eq. 2, reduces the number of collected events, n, and therefore the SNR. Thus once more, the key to reducing scan length or radiation dose, without sacrificing image quality, has to be through increasing n by maximizing the product $G\varepsilon^2$ and by improving the timing resolution Δt.

Limitation 4: Cost

PET is commonly considered to be an expensive diagnostic tool. The cost for utilizing PET in a research or healthcare setting is a complex function of several factors, of which the cost of the actual instrument is just one. Nonetheless, reducing the cost of the scanner is likely to be beneficial for the broader application of PET. However, referring back to Eq. 2, reducing the cost of the scanner without sacrificing SNR is challenging.

The cost of a scanner, to first order, is related to the cost of its components, which, for a given bore size, mostly scales with the degree of geometric coverage, G. A scanner that covers twice the solid angle around the patient, assuming a fixed detector ring diameter, will require twice as many detectors and twice the number of channels of electronics. Thus, increasing G typically increases cost, while decreasing G decreases SNR. The key therefore for reducing cost while maximizing geometric sensitivity is likely through the development of detector materials that are more efficient and cost less for a given thickness. For example,

if a new material could achieve the same efficiency ε as current state-of-the-art scintillators, but does so with 80% of the volume and is 20% cheaper, the material costs would be reduced to $(0.8)^4 = 0.41$ of the original amount without sacrificing intrinsic efficiency ε. Thus a 60% savings in the most expensive components of the scanner might be realized by newer materials that have higher stopping power and use cheaper raw materials, or involve lower manufacturing costs (for example lower temperature or faster material growth). Another approach to reducing cost while maintaining current levels of SNR is to improve the timing resolution. Improvements in timing resolution could be traded off for less detector material (lowering G and/or ε), as long as the factor $G\varepsilon^2/\Delta t$ is maintained.

The common theme critical to addressing the first three limitations is to find ways to increase the term $G\varepsilon^2/\Delta t$ in Eq. 4. If this can be done, then it can directly lead to better SNR, or, alternatively, current levels of SNR could be maintained but with shorter scan times, or at lower radiation doses. To reduce cost without negatively impacting SNR, either the time-of-flight capabilities need to be improved without the use of more expensive components, or more efficient and/or lower cost detector materials per unit thickness need to be used.

Given these considerations, it now becomes clear why innovations in PET instrumentation are focused on optimizing the scanner design to achieve higher detection efficiency in various imaging tasks (e.g. whole-body imaging and dedicated organ imaging), and advancing detector technology to achieve superior timing resolution. These approaches are essential for realizing the full potential of PET. In addition, relevant efforts continue to address improvements in detector and system spatial resolution, as well as energy resolution. Finally, the investigation of detector materials that can produce the same SNR at a lower cost, will likely be important to further broadening the impact of PET.

3. PET Scanner Designs

Almost all human PET scanners currently sold are largely designed around the main clinical task of PET, namely cancer staging and monitoring response to therapy using the radiotracer ^{18}F-fluorodeoxyglucose (FDG). Typically an “eyes-to-thigh” scan covering 100–120 cm of the body is acquired using a series of overlapping bed positions, or continuous scanning of the bed through the PET camera (Figure 1a). These PET scanners use very efficient detectors, typically 18–25 mm thick crystals of lutetium (yttrium) oxyorthosilicate (L(Y)SO) or bismuth germanate (BGO) scintillators that result in detection efficiencies (ε in Eq. 4) of 80–90%, and time-of-flight capabilities of ~400 ps or better with lutetium-based scintillators. These scanners are integrated with CT or MRI scanners to provide registered anatomic information in the same scan. Current designs represent one small region in the available parameter space, specifically a particular balance between materials cost and the geometric coverage G. Several recent initiatives are questioning this choice and examining the effect of developing scanners with much higher values for G.

There also is significant interest in developing dedicated PET imaging systems, for example for brain and breast imaging (Figures 1b and 1c), that optimized for imaging those specific organs. While a range of innovative and high-performance systems have been developed, the challenge is to build sufficient patient volumes (by demonstrating substantial clinical or

research benefit) to justify the development of dedicated systems and support commercial viability of these products.

There also has been a long history of using PET in preclinical research [9, 22, 23]. There is significant overlap in the requirements for brain imaging in humans and nonhuman primates, and a significant industry has grown up around very compact PET systems for preclinical studies in rodents (Figure 1d), typically aimed at evaluating the pharmacokinetics or treatment effects of new therapeutics, or in aiding the development of new radiotracers. These small-scale systems also have been an excellent testing ground for new advanced detector technologies, especially those pushing the barriers for spatial resolution.

3.1. Extended axial field of view and total-body PET

A typical whole-body clinical PET scanner covers 20–25 cm of the body axially at any one time. Thus, only about $1/8^{th}$ of the body is actually in the field of view of the scanner. Furthermore, the average detection sensitivity for activity within the scanner field of view is on the order of just 2.5% (due to the isotropic emission such that many photon pairs do not intercept the detectors). Thus the overall detection efficiency is about 0.3% [21]. Thus ~99.7% of the emitted photon pairs go undetected. Examining Eqs. 2 and 4, it is easy to see a pathway to large increases in n, and therefore SNR, for the task of whole-body imaging. By using more detectors and extending the scanner along the length of the body, the factor G can be increased dramatically. Computer simulations of a total-body scanner (Figure 1e) have shown that a scanner with an axial length of around 200 cm will detect ~40 times more events (even after correcting for increases in random and scattered coincidences) for the same activity and imaging time compared to a scanner with an axial length of 22 cm [24, 25]. Even for the scan of a single organ, for example the heart, which can be imaged in a single bed position with current scanners, this extended geometry will result in a 4-5-fold increase in the number of detected events.

A factor of 40 gain in G and thus the number of events detected would represent a significant step in addressing many of the limitations of PET identified earlier in the context of whole-body FDG imaging. For example, without increasing the dose or scan time, Eq. 4 estimates and computer simulations confirm [26] that the SNR would be increased by a factor of ~6.6. With much better statistical quality data, it would be possible to use higher spatial resolution detectors and get closer to approaching the actual physical resolution limits of PET. Major improvements in SNR and spatial resolution, one can argue, should permit the detection of smaller or less metabolically active cancerous lesions, as well as better quantification of tracer uptake, or changes in tracer uptake following treatment, in lesions. Alternatively, if current diagnostic images provide sufficient SNR for a given clinical task, the 40-fold gain in G could be used to reduce the imaging time or injected activity by a factor of 40 while maintaining the same SNR as currently achieved. Thus, PET scans of the entire body could be achieved potentially in 15–30 seconds rather than 10–20 minutes, or for an effective radiation dose of 0.15–0.2 mSv rather than the 6–8 mSv common today. To put this in context, this effective radiation dose is similar to that of a standard 2-view chest x-ray (~0.1 mSv).

The only, but not insubstantial difficulty, of implementing this approach are fears concerning cost. Clearly, a scanner that uses on the order of 8 times more detector material to cover the total-body, will cost considerably more. However, cost always has to be evaluated in the context of benefit, and the benefits cannot be quantified without data. Thus, a number of initiatives have been launched that will begin to address this question. The EXPLORER consortium, led by the University of California, Davis, is currently completing the first total-body PET system (Figure 2) which will have an axial extent of 195 cm [27, 28]. There also are parallel efforts at the University of Pennsylvania [28–30] and the University of Ghent [31], to develop systems in the range of 100–140 cm in axial length combined with very good timing resolution to further boost SNR. These efforts will allow the trade-offs between geometric coverage, timing resolution and cost to be explored, and provide data from a completely different parameter space than has been possible to date. The impact on diagnostic and research PET studies, and whether this results in changes to the design of future generations of commercial PET scanners, remains to be determined, but of all developments in PET at the present time, these efforts have the highest potential to make a very large difference by directly addressing the key performance limitations of current PET systems.

3.2. Time-of-flight PET

Improvements in timing resolution are an important pathway to realizing higher SNR, and this has been the area of greatest improvement in the past 5 years in clinical PET systems. The routine use of bright and relatively fast lutetium-based scintillators, high-speed and sensitive photodetectors, along with fast and stable electronics, has been the foundation for the successful introduction of time-of-flight capability in commercial scanners and subsequent improvements from the 500–600 ps timing resolution of the earliest systems to well under 400 ps for the very latest generation systems [17, 18]. Further developments at the detector, electronics and systems levels strongly suggest timing resolution will continue to improve, probably to the 200–250 ps range in the relatively near term. Beyond that, a combination of the rate of scintillation light production and the response speed of the photodetector become limiting factors, however, major efforts are underway in research laboratories, that offer possible pathways to reaching 100 ps or even beyond in the future [32].

These improvements in timing resolution, can be combined with the geometric enhancement described in the previous section. Together, they provide the opportunity to achieve an order of magnitude gain in SNR ($\sim\sqrt{40}$ for total-body coverage $\times$ $\sim\sqrt{2.5}$ for timing) for whole-body imaging. This would represent an enormous performance change with the potential for major benefits in diagnostic care and clinical research.

3.3. Brain Imaging Systems

The large and increasing economic burden of neurodegenerative disease in an aging population, along with the availability of specific radiotracers for the amyloid and tau pathologies associated with Alzheimer's disease and the reduced dopamine synthesis capacity in Parkinson's disease, argue for the importance of developing high performance brain imaging systems. The opportunities have been known for some time, and PET and

PET/MRI systems with more optimized geometries for imaging the human brain have been developed [33–35]. Specifically, smaller diameter rings of detectors can be used and good solid angle coverage of the brain obtained using smaller amounts of detector material compared to a whole-body scanner, thus improving SNR while not necessarily increasing cost. Some researchers are investigating the use of additional detectors under the chin and by the ears to further increase geometric coverage and thus SNR [36, 37]. The demands for high spatial resolution are perhaps more acute in the brain, as there are many fine structures of interest and the limited resolution of PET leads to significant partial volume errors that influence accurate quantification. While a smaller diameter detector ring suitable for the size of the head reduces the non-colinearity effect, and offers the prospect of ultimately achieving 1–2 mm spatial resolution, the reduced ring diameter also increases the so-called *depth-of-interaction* effect. This can lead to a degradation in spatial resolution due to the variable depth to which photons can penetrate into the detector material before interacting. Reducing or eliminating this effect requires detectors with depth-encoding capabilities [38]. Furthermore, the level of timing resolution that can now be achieved in PET suggests that there may be value in incorporating time-of-flight information into dedicated brain systems as well.

To date, no system has been built that combines the necessary intrinsic detector spatial resolution, depth-of-interaction encoding, timing resolution and detector efficiency in a compact geometry to fully realize the combination of SNR and spatial resolution that should be achievable. For hybrid systems, there is a clear advantage in the setting of the brain to combine dedicated brain PET systems with MRI, rather than CT, as the soft tissue contrast excellent and there is no radiation dose associated with MRI. Thus, most technology developments for dedicated brain PET systems use a technology platform that can be MRI-compatible.

Because brain imaging often is closely linked with behavioral tasks or other monitoring, there has been interest in developing novel PET systems which allow for scanning in a more natural setting, for example sitting upright [35, 37] or even while freely moving with a wearable system [36, 39]. The latter is complicated due to the weight of the detector materials in a highly efficient PET scanner, and the range of possible head motions. Nonetheless, with careful mechanical design, and some motion constraints or tracking abilities, such approaches likely are technologically feasible. The future of these developments will depend on the impact of these innovations in opening up new areas of research or clinical care.

Instrumentation for dedicated brain PET scanners is an active area of research, however, developments have perhaps been somewhat impeded by doubts concerning the ultimate clinical role and commercial viability of a dedicated brain scanner. It also is worth noting that clinical brain imaging systems also could play an important role in pre-clinical imaging. A significant number of PET neuroimaging studies are conducted in nonhuman primates, and a high performance human brain scanner also would serve as an excellent platform for preclinical research in these important model systems.

3.4. Breast Imaging Systems

Another highly relevant target for dedicated imaging systems is the breast [40]. Early detection of breast cancer and the ability to image therapeutic response and recurrence are among the applications where dedicated PET imaging could help, especially given the high false positive rate of screening mammography using x-rays. While PET is likely to remain too expensive for routine screening, secondary screening following an abnormal mammogram, or screening in populations at high risk of breast cancer due to genetic factors may be viable applications. Quantitative assessment of response to neoadjuvant chemotherapy, and detection of recurrence in the presence of scar tissue from prior surgery also offer opportunities for dedicated breast PET imaging. A variety of systems dedicated to breast imaging have been developed [41], some based on positron emission mammography (PEM) which use limited angle information from a pair of parallel plate detectors [42–44] to fully tomographic systems [45–47], including hybrid breast PET/CT scanners [48]. Commercial systems have been developed and used in clinical trials, but to date these have not led to implementation of dedicated breast PEM or PET in standard-of-care.

The challenges and approaches from an instrumentation perspective are very similar to brain imaging. Detector plates or rings of detectors are brought close to the breast to achieve high solid angle coverage and efficiency with relatively small detector volumes, improving SNR and reducing cost compared to breast imaging on a standard whole-body PET scanner. The reduction in non-colinearity and the higher SNR also offers opportunities for increasing spatial resolution by using very small scintillator crystals or slabs of continuous scintillators (so called monolithic detectors) read out by an array of photodetectors. However, to approach the limiting resolution, while maintaining very high efficiency, depth-of-interaction encoding detectors will ultimately be required. One geometric challenge for breast imaging is imaging in the region close to the chest wall. In a dedicated breast PET scanner, this region inevitably falls at the very edge of the field of view of the scanner where the geometric collection efficiency is very low. Indeed, careful design of the patient couch and engineering of the detector system to be able to image right up to the edge of the couch without space for significant shielding of the detectors from activity in the rest of the body are key to even being able to image the region within 1–2 cm of the chest wall at all.

Similar to brain imaging, the ultimate system that approaches the limiting values for detection efficiency and spatial resolution has yet to be developed, but further large investments in R&D necessary for that development are hampered by the uncertainty regarding the ultimate applications and adoption of the technology.

3.5. Preclinical Imaging Systems

Probably the most successful example of dedicated PET systems have been those designed for small-animal (mouse and rat) preclinical studies [9, 49]. Several hundred systems are installed in research laboratories, contract research organizations and pharmaceutical companies around the world and are used to evaluate the pharmacokinetics and pharmacodynamics of new therapeutic entities such as small molecule drugs, antibodies, cell-based therapies and nanoparticles. Often, these systems also are integrated with high resolution microCT or preclinical MRI systems [23, 50].

The design trade-offs and priorities in this application are somewhat different than clinical imaging, with a premium on achieving significantly better spatial resolution given the small volumes of the organs and tissues of interest. However, as explained earlier, high SNR is still a necessary foundation, in order to provide sufficient counting statistics to reconstruct images using much smaller voxel sizes. One advantage is that there is less absorption and scatter of the signal within the body, increasing the number of photon pairs that escape and are available for detection (thus increasing the value of *k'* in Eq. 4). SNR in rodent studies is also increased by using a higher injected activity per unit body weight compared to a human study. For example, typical injected activities in a mouse are approximately 100-fold less than in a human (100 μCi (3.7 MBq) in a mouse versus 10 mCi (370 MBq) in a human), but a typical mouse weighs ~2500-fold less than a human. Even higher injected activities have been used to further boost SNR, however, with many radiotracers, care must be taken to keep the injected mass low so that the study is still a tracer study and there are no mass effects. Radiation dose effects also should be considered in a longitudinal study that might involve multiple radiotracer administrations.

For the reasons described above, it is relatively easy to achieve relatively high SNR in small-animal imaging when using a compact geometry that surrounds the subject with efficient detectors. This opens the door to explore a range of detector approaches that can achieve much higher spatial resolution (0.5–1 mm or so) and may also encode depth-of-interaction information [38] to give very uniform spatial resolution across the entire imaging volume. It has been demonstrated that a spatial resolution of around 0.5–0.6 mm is possible in small-animal systems, and approaches using very tiny scintillator elements (down to 0.5 × 0.5 mm in cross-section) [51] as well as monolithic detectors [52] are being pursued.

One serious challenge, especially related to molecular neuroimaging, is the effect of anesthesia on radiotracer uptake and distribution. Furthermore, anesthesia precludes direct temporal correlation of animal behavioral data with PET imaging studies. For these reasons, efforts also have been devoted to developing approaches that permit brain imaging in awake rodents, either by using a very compact scanner that can be affixed to the head of the animal [53] or by using a motion tracking system to monitor head position during imaging [54]. Both these approaches are challenging for different reasons, nonetheless working prototypes have been developed in the research setting.

Because of the relatively small number of detector elements, photodetectors and channels of electronics required to produce high-quality images in this application, and its widespread adoption, small-animal PET also serves as an excellent initial testing ground for new PET instrumentation approaches and technologies, for example new scintillators, direct semiconductor detectors, new photodetectors, electronic read out and computational event processing strategies, and detectors suitable for use in hybrid PET/MRI systems. Thus, much innovative detector development (see Section 4) is focused around this application [55]. The only major exception relates to work on fast timing, as time-of-flight PET only starts to become relevant when the timing resolution corresponds to a distance that is less than the diameter of the object being imaged. For a mouse, which measures ~1.5 cm across the width of its body, a timing resolution of better than 100 psecs would be needed before any consideration of adding time-of-flight information would be warranted.

3.6. Other PET Systems

Specialized PET systems also are under development for several other applications. One with particular promise are in-beam PET systems used for monitoring proton or heavy ion therapies. There is a significant expansion in the clinical use of proton therapy, in particular, where range verification is quite critical. As protons or heavy ions pass through tissue, they participate in nuclear reactions, generating short-lived positron-emitting species that can be imaged [56]. The challenges, however, are quite formidable, as the signals are low, rapidly decaying, and the detection system must work in a high background radiation environment consisting of neutrons and gamma rays. Several research groups are pursuing the design and development of such systems [57–60].

A second area that has attracted interest, especially with the emergence of new radiotracers that bind specifically to prostate specific membrane antigen (PSMA) [61], are PET systems optimized for prostate imaging. Approaches range from a fairly straightforward geometric optimization of a whole-body design [62], to the development of endorectal detectors that can be placed in coincidence with external rings of PET detectors to achieve high spatial resolution and sensitivity at the prostate [63]. A more generalized concept of using compact high-resolution detectors placed close to an organ of interest, and operating in coincidence with standard whole-body PET scanners to achieve high local resolution and sensitivity, is being examined for a range of applications, including breast imaging [64].

Outside of biomedical research, an area that has received some recent attention is the use of PET to image plant physiology and metabolism. The ability to track carbon, as well as transport of nutrients, salts and heavy metals in plants has a range of applications including research related to crop yields, salt-tolerance and soil remediation. Dedicated PET systems, integrated with environmentally-controlled growth chambers, have been developed for these applications [65–67], but to date deployment is limited to a very small number of institutions that have active plant research programs as well as expertise and infrastructure for PET instrumentation and radiotracer production.

4. Detectors

The detectors in a PET scanner perform a central role in the system as they are responsible first for absorbing the 511 keV photons, and second, for providing accurate information describing the position-of-interaction, the energy of the detected photon, and the time-of-interaction, all of which are crucial factors affecting the overall sensitivity, spatial resolution, capability for rejecting random and scatter events, and time-of-flight capabilities of the scanner. Therefore, many of the innovations in PET instrumentation focus on developing new detector technology either for broad application (e.g. brighter and faster scintillators, more sensitive photodetectors), or for specific imaging systems (e.g. very fast detectors for clinical time-of-flight systems, high spatial resolution detectors for pre-clinical imaging).

A typical PET detector (Figure 3) is comprised of an array of scintillator crystals, each measuring ~ 4 × 4 × 20 mm in size for clinical systems, and ~1 × 1 × 10 mm for pre-clinical systems, coupled to a set of photodetectors such as silicon photomultipliers (SiPMs) or photomultiplier tubes (PMTs) via a thin light guide [68]. Two notable exceptions to this

common detector design are one-to-one coupling, in which the individual crystals are directly coupled to individual photodetectors [69, 70], and monolithic detectors, where a large (i.e. 30 × 30 × 20 mm) continuous scintillator block is coupled to an array of photodetectors [71, 72]. Lutetium-based scintillators, such as LSO or LYSO, are used in nearly all modern systems because of their favorable combination of high stopping power, good luminosity, and short decay time, resulting in high sensitivity, fast timing resolution, reasonable energy resolution, and low dead-time [73]. SiPMs are now the photodetector of choice for modern PET detectors, owing mainly to their compact size, magnetic insusceptibility (making them compatible with hybrid PET/MRI systems), high photon detection efficiency (PDE) and low timing jitter [74], and have essentially replaced PMTs in both clinical and pre-clinical systems. SiPMs are a type of solid-state detector made up of several thousand individual microcells, each of which discharges an avalanche of charge ($\sim 10^6$ amplification) in response to a detected optical photon, and is therefore capable of detecting individual photons [75]. The microcells are typically connected in parallel such that the output represents the number of fired microcells, and can therefore be used as photon counting devices. One unique SiPM device is the so-called digital SiPM [76, 77]. In these, each microcell is integrated with logic circuity to enable readout of individual microcells. This has a number of practical benefits, such as the ability to disable exceptionally noisy microcells, and flexible digital processing circuits to optimize performance, especially timing.

The light produced in a scintillator crystal is typically spread across multiple photodetectors through the light guide, and the spatial distribution of light measured by the set of photodetectors, that is, the amount of light collected by each photodetector is used to determine the crystal in which the 511 keV photon was absorbed (i.e. the position-of-interaction in the detector). The total amount of light collected by all photodetectors is used to estimate the energy of the absorbed photon. Lastly, the time-of-interaction is estimated from the rising edge of the photodetector signal, or waveform, and is therefore influenced by the properties of the earliest arriving scintillation photons. Simple signal processing techniques such as leading edge discrimination (the time-of-interaction is estimated as the time the waveform crosses a voltage threshold), or constant fraction discrimination are normally then used to estimate the time-of-interaction, either from the analog signals or from digitized waveforms.

It is clear that all of the information describing the 511 keV photon's position-of-interaction in the detector, the amount of energy deposited in the detector, and the time-of-interaction of the 511 keV photon in the detector, is contained in the spatial and temporal properties of the detected scintillation light and the resulting electrical signal from the photodetector. Therefore, the major trends in detector development generally involve improving the generation and collection of scintillation light with new scintillators and photodetector technology (mainly SiPMs), optimizing the detector configuration to make better use of scintillation light, and developing new signal processing algorithms to make better use of the information contained in the photodetector waveforms.

A further trend is to explore and develop non-scintillation mechanisms for radiation detection, for example the use of direct detection inside semiconductor materials such as

CdZnTe (CZT) [78], mainly for high spatial resolution applications. Direct semiconductor detectors bypass the relatively inefficient process of converting the 511 keV energy to optical photons in a scintillator, and instead use a dense, high atomic number semiconductor crystal to directly absorb and convert the 511 keV photon into a large number of electron-hole pairs. Electrodes placed across the semiconductor are then used to supply a large electric field in order to collect the electric charge.

4.1. Time-of-Flight Detectors

The most significant recent development in PET detector technology has been the major improvement in timing resolution, mainly as a result of advances in scintillator materials, photodetectors (SiPMs), and faster electronics [79, 80]. First, it is important to discuss the physical factors that influence timing resolution in a PET detector to provide the relevant context for discussing detector innovations [32].

Following the absorption of a 511 keV photon in the detector, several thousand scintillation photons are generated in the crystal via recombination of electrons and holes, and emitted following the scintillator's rise and decay times. Both the total number of photons as well as their emission times are random processes, defined by the approximately Poisson statistical randomness inherent to scintillators. The isotropically emitted scintillation photons then propagate through the crystal, where they are ultimately either absorbed in the crystal, or lost through the top or sides of the crystal, or, ideally, exit the crystal and enter the photodetector. The loss of photons in the crystal also introduces larger statistical fluctuations in the scintillation light, and the variable propagation times of each photon adds further variance in photon detection time. The photodetector collects the scintillation light and converts a fraction of the photons to electrical charge. The process associated with converting the photon energy to electric charge is also a random process, first by the probability of absorbing an incident photon and converting to electric charge, and second by the generation and collection of charge carriers over a short period of time (i.e. electrons and holes in an SiPM), and this timing jitter also adds variance in the detected arrival time. Lastly, the electrical signal from the photodetector is typically passed through circuitry to amplify the signal and an application-specific integrated circuit (ASIC) or field programmable gate array (FPGA) is used to estimate the time-of-interaction from the signal.

Obtaining a precise estimate of the time-of-interaction in the detector thus relies on minimizing the variance in the detection times of the earliest photons. This includes generating and collecting as much scintillation light as possible, reducing the rise and decay times to increase the early photon flux, minimizing the spread in propagation times in the crystal, and preserving the timing properties of the detected photons after electrical conversion in the photodetector. Progress in these areas represents most of the significant developments in time-of-flight PET detector technology.

4.1.1. State of the art time-of-flight detectors—The development of fast, bright, and efficient Lu-based scintillators, in particular LSO/LYSO, enabled the re-birth of time-of-flight PET ~10–15 years ago, resulting in state-of-the-art scanners providing time-of-flight capabilities of ~ 500 ps [81–83]. LSO/LYSO is still used in nearly all modern time-of-flight

whole-body scanners, but several systems now achieve < 400 ps time-of-flight capabilities, some of which employ detectors with timing resolution reaching <250 ps [70, 84–86]. In addition, bench-top detectors using similar materials can now achieve < 80 ps timing resolution with optimized detector configurations and short scintillator crystals and <140 ps with longer crystals [87–89]. So the question is, what has enabled this massive improvement in timing resolution in recent years?

The most significant technology enabling the shift in timing resolution has been the rapid development and maturation of SiPMs. Historically, fast photomultiplier tubes (PMTs) were used in PET detectors owing to their relatively low noise, fast response, and high sensitivity compared to other technologies. However, following 10 – 15 years of development, SiPMs now provide exceptional PDE, fast timing response, and low noise properties [76, 90]. This has resulted in nearly all manufacturers shifting to the use of SiPMs in modern time-of-flight scanners.

The main benefit of SiPMs for time-of-flight applications is their high PDE. Whereas PMTs were limited to ~ 25% PDE, modern SiPMs can provide > 40% PDE for scintillation light, and are therefore much better suited to collect as much of the early scintillation light as possible. Additionally, SiPMs provide low timing jitter, mainly as a result of mainly as a result of operating the SiPMs in the avalanche regime and the narrow amplification region within the silicon where the signal is produced, and are therefore better suited to preserve the fast timing properties of the early scintillation photons.

In addition, the compact physical structure of SiPMs is beneficial for more efficiently collecting the scintillation light in a light-sharing PET detector. PMTs that were previously used in PET detectors were most often circular, which resulted in large gaps between PMTs in a PET detector module, and ultimately poor collection of scintillation light. Square SiPMs can be packed more tightly together, resulting in overall higher geometric efficiency. Previously, the packing fraction of SiPMs was limited by the space needed for electrical contacts on the sides of the devices, resulting in minimum ~ 2 mm gaps between sensors. However, modern SiPMs employ through silicon via (TSV) technology, in which the electrical contact passes through the center of the sensor, allowing essentially negligible dead-space between adjacent SiPMs [91]. The compact size and magnetic insusceptibility of SiPMs also facilitates the construction of very compact detector rings that can be integrated within the bore of MRI scanners for simultaneous PET/MRI imaging [92–94].

One of the previous limitations of SiPMs for fast timing resolution was their noise properties. These solid-state devices typically exhibited much higher random “dark” noise compared to PMTs, which confounded the early scintillation signal for timing. In addition, SiPMs also exhibit correlated noise, such as optical cross-talk and after-pulsing. However, significant efforts into optimizing the SiPM material properties and physical structure have largely reduced these noise sources, leading to their use in state-of-the-art time-of-flight detectors and ultimately their adoption in commercial scanners.

4.1.2. Frontiers and Innovations in Time-of-Flight Detector Technology—The limit of achievable timing resolution in PET detectors continues to steadily progress to well

below 100 ps in optimized bench-top settings [79, 80]. Research in this area has mainly focused on the following topics: (1) increasing the early photon flux with brighter and faster scintillators and optimizing the light transport in the crystal, (2) improving the timing properties of SiPMs, (3) developing advanced electronics and signal processing methods to better extract the time-of-interaction from the SiPM signal, and (4) investigation into alternative methods to traditional scintillation-based timing to estimate the time-of-interaction [32].

4.1.3. Scintillators—There have been a small number of developments in scintillator technology for time-of-flight, many of which are based on derivatives of the commonly used Lu-based scintillators (LSO or LYSO). One avenue to improve the timing performance of Lu-based scintillators has been through the use of co-doping with alkaline metals. LSO and LYSO are typically doped with Ce^{3+}, but recently it has been shown that co-doping with Ca can slightly reduce the rise time, and shorten the decay time from 42 ns to ~32 ns, leading to improved timing resolution, as low as 73 ps for 3 mm long crystals and 117 ps for 20 mm long crystals [88, 89, 95, 96]. A similar scintillator has been developed by Zecotek, LFS-3, which provides similar light output to LSO/LYSO but with shortened decay time of 36 ns leading to small improvements in timing resolution [97]. Another promising Lu-based scintillator for time-of-flight is LGSO [98]. Although this scintillator typically suffers from slightly lower total light output compared to LYSO, it has ~ 30% faster decay time which improves the early rate of scintillation light. Timing resolutions of 80 ps with short crystals and 122 ps with 20 mm long crystals have recently been measured with LGSO [87]

The high cost of the raw materials and fabrication process for current Lu-based scintillators is a major factor to the overall cost of PET systems, therefore there is an active search for alternative scintillators that can provide similar detection efficiency and timing resolution at lower cost. Some of the most promising alternative scintillators with overall attractive properties similar to LYSO are the recently developed cerium-doped rare-earth garnets (GAGG, GGAG, GluGAGG) [99, 100]. Compared to LSO/LYSO, these scintillators provide overall higher light output, but with slightly longer decay time and somewhat lower detection efficiency. Fast timing resolution has been achieved with these scintillators [88, 101, 102], however, the relatively long decay time currently limits the potential of these scintillators to reach state-of-the-art timing resolution provided by LYSO. However, a practical benefit of these garnet scintillators is the ability to fabricate using ceramic techniques, leading to simplified detector fabrication and lower cost compared to the crystal growth methods necessary for most Lu-based scintillators, making these scintillators potential candidates for low-cost systems with modest timing resolution. Recently however, an Lu-based scintillator, Lu_2O_3, has been developed with suitability for ceramic manufacturing, along with an extremely fast decay time of ~1.5 ns, [103, 104], suggesting potential use for low-cost, high sensitivity time-of-flight detectors.

Halide scintillators such as $CeBr_3$ and $LaBr_3$ scintillators provide very good properties for fast timing resolution [105–109]. The light output of these is ~2–3 fold higher than LYSO, and has a primary decay time of ~16 ns, resulting in ultra-fast timing resolution, as good as ~ 75–80 ps in recent experiments with fast SiPMs [110]. However, apart from these ideal scintillation properties, $LaBr_3$ and $CeBr_3$ suffer from much lower stopping power compared

to Lu scintillators. The lower sensitivity can be offset by using longer crystals, but this results in poorer spatial resolution due to depth-of-interaction effects, and introduces larger variability in scintillation light propagation time that offsets the intrinsically fast timing properties of $LaBr_3$ and $CeBr_3$. Because of these, in addition to the hygroscopic nature of halide scintillators, $LaBr_3$ and $CeBr_3$ have only been used in research systems [110, 111].

In a conventional PET detector using a pixelated scintillator array, the long finger-like crystals introduce long optical path lengths and many reflections for the scintillation light, which ultimately adds significant variance to the earliest timing information. Of course, the easiest way to overcome this is to use shorter crystals [112], but this comes with a substantial reduction in detector efficiency (ε in Eq. 4), and is therefore not justifiable for whole-body scanners where SNR already is a limiting factor. In thick scintillator crystals, various strategies have been investigated to improve the light transport within the crystal, such as optimizing the crystal's surface finish and the inter-crystal reflector [113], and improving the extraction of scintillation light from the crystals using nano-structured materials such as photonic crystals [114]. Additionally, the light collection efficiency can be improved by modifying the detector configuration, such as by placing SiPMs at both ends of the scintillator in the so-called "dual-ended readout" scheme to reduce the overall propagation distance of scintillation light before collection [115, 116]. Alternatively, monolithic detectors provide a convenient solution for improving light transport because of the larger crystal volume and absence of inter-crystal boundaries. Recently, investigators have combined monolithic detectors with dual-ended digital SiPM read-out to obtain an outstanding timing resolution of 147 ps with a 22 mm thick LYSO crystal, compared to 214 ps with single-ended readout [117].

4.1.4. Photodetectors—The development of the SiPM has been a key contributor to recent improvements in PET detector timing resolution. Compared to the PMT, SiPMs boast up to two-fold higher efficiency in collecting scintillation photons and typically lower timing jitter, but exhibit higher dark noise and correlated noise such as afterpulsing and optical cross-talk [118]. Although the limiting factor for timing resolution is largely still dominated by the scintillator physics and light transport in long crystals, there is room to improve the SiPMs intrinsic timing performance, and this will become especially important in improving the timing resolution beyond 100 ps. The factors currently limiting the SiPMs intrinsic timing resolution are PDE, noise, electrical capacitance, and timing jitter. The influence of PDE is relatively straightforward; a higher probability of collecting and detecting the early scintillation light leads to improved timing performance, similar to the effect of increasing light output in a scintillator. SiPMs have traditionally been characterized by lower PDE at shorter wavelengths (i.e. 400 nm) compared to longer wavelengths (500 nm) which is problematic for scintillators such as LYSO that have their peak emission at ~420 nm. Recently, SiPMs have been developed with significantly higher sensitivity for blue light, providing up to 55% PDE at 420 nm [119, 120].

However, one of the main limiting factors affecting SiPM PDE is the dead-space around microcells. To maximize efficiency, large microcells (e.g. 100 μm) minimize the dead-space between adjacent microcells, however, the trade-off associated with this in terms of timing is increased capacitance which slows down the rising edge of the pulse. This leads to larger

variance in the timing pick-off in the presence of electronic noise, degrading timing resolution. To counteract this trade-off and make use of the beneficial timing properties of smaller microcells, an active area of SiPM development has been in the fabrication process to reduce the gap between SiPM microcells while minimizing noise (optical cross-talk generally increases with smaller microcell gaps) [120, 121].

The intrinsic timing response of the SiPM, often called the single photon timing resolution, also influences the overall timing resolution of the detector, albeit on a smaller level than the scintillator contribution and the PDE. The intrinsic timing response of an SiPM is a complex function of the variance associated with the charge amplification in the silicon, random and correlated noise in the SiPM, electrical noise in the read-out circuit, and variations in the timing response of different microcells. Most importantly, this factor is dominated by the size of the SiPM: for example a 3×3 mm^2 SiPM has an intrinsic timing resolution of 180 ps, while the same microcells but packaged in 1×1 mm^2 size produces an SiPM with an intrinsic timing resolution of 100 ps [122, 123]. Taken to the extreme, a single microcell can achieve intrinsic timing resolution of < 50 ps, and as low as 20 ps in recent developments [124]. Experiments have shown that the main reason for degraded timing resolution with larger area SiPMs are again, the higher capacitance, which slows down the timing response of individual microcells, variations in signal propagation time from the microcells to the timing circuitry depending on their relative position in the SiPM, and higher noise with increasing device size [122]. In the larger area devices (3×3 mm^2 or 6×6 mm^2) that are commonly used in PET systems for cost-effectiveness, noise is typically the dominating factor in determining an SiPM's single photon timing resolution.

One promising route to improve SiPM intrinsic timing resolution is to parallelize the readout of all microcells and incorporating timing circuitry for each individual microcell (or small regions of microcells) [125, 126]. Although the timing performance of the entire SiPM would still be affected by other sources such as optical cross-talk and PDE, this type of readout would be highly beneficial in supporting further improvements in timing resolution. The main challenge here is implementing this readout without strongly impacting SiPM PDE by introducing more dead-space between microcells. Digital SiPMs are intrinsically capable of integrating a large number of timing channels and several strategies have been investigated in this regard [127], but currently this has not been fully realized due to the loss in PDE which negates the improvement in timing resolution offered by individual timing circuits. However, this can be expected to change with advances in device fabrication.

4.1.5. Signal processing—Given that the signal from the detector contains all the information describing the time of interaction in the scintillator, an important feature of the detector is the signal processing method used to extract the time-of-interaction. Traditionally, both in commercially available scanners and in many research settings, the waveforms from the detectors are amplified and passed through an ASIC or FPGA, which applies a leading edge or constant fraction discriminator to estimate the time of interaction with high precision timing circuitry [128–131]. These methods have shown good performance for timing with SiPMs, but are often costly to develop and are generally tailored for a narrow range of detector configurations. As SiPM technology continues to evolve, for instance with the potential to read-out timing information from individual

microcells, it is likely beneficial to implement statistical signal processing methods to make better use of the timing information that represents the random nature of scintillation detection. One example of this is the use of maximum likelihood estimation or a weighted average estimator to estimate time-of-interaction using multiple time stamps for each event [132, 133]. Improved timing resolution has been shown in a monolithic detector by modeling the randomness in each time stamp due to photon counting statistics as well as differences in photon travel time from the site of interaction to each SiPM.

Alternatively, and possibly complementary to these maximum likelihood estimators with multiple time stamps, are efforts to better extract timing information from digitized detector waveforms, recently made possible with affordable fast digitizing hardware [134]. In the conventional timing discrimination methods such as leading edge threshold, all the timing information contained in the detector signal is essentially condensed into a single estimate, most simply as the time that the signal crosses a voltage threshold. The efficient use of these simple signal processing methods then requires extensive optimization to the readout circuits for the SiPMs in order to reduce noise and maximize the slope of the signal. An alternative approach is to implement statistical estimators directly on the detector waveforms to make better use of the timing information contained in the signal. Maximum likelihood estimation methods have been proposed, where each digital waveform sample is used in a maximum likelihood estimator resulting in improved timing resolution especially at relatively slow sampling rates [135]. Recently, we demonstrated the application of convolutional neural networks to estimate time-of-flight directly from the pair of digitized waveforms from a coincidence event, demonstrating >20% improvement in timing resolution compared to leading edge or constant fraction discrimination [136]. This neural network approach does not require a statistical model of the timing properties of the detector signal, conversely it learns features of the signals that relate to the ground-truth time-of-interaction that can readily be obtained experimentally.

4.1.6. Alternative timing methods—The process of producing scintillation light in the crystal begins with a complex random process of generation and relaxation of electron-hole pairs (resulting in the scintillator's rise time e.g. ~75 ps for LYSO [96]), and ultimately this process introduces randomness in the generation times of the earliest photons [32]. This means that for scintillators with non-negligible rise time the scintillation process imposes a limit on timing resolution, and therefore an alternative approach is likely needed in order to achieve ultimate timing resolution of ~10 ps. One possible method is to make use of Cerenkov light rather than scintillation light for timing [96, 137, 138]. When a 511 keV photon is absorbed in the crystal, several high energy electrons are produced, and transiently travel faster than the speed of light in the crystal media for a brief time, during which Cerenkov light is produced. Since this Cerenkov light is produced essentially instantaneously with the 511 keV photon absorption, there is little variance in the production times of the Cerenkov photons relative to the 511 keV photon's time of interaction in the crystal. To make best use of this mechanism, the crystal medium should have high refractive index and high photofraction to maximize the number of Cerenkov photons produced, as well as high transparency for the blue light characteristic of Cerenkov emissions.

Initial studies of this method involved non-scintillating Pb-based crystals (PbF_2) and timing resolutions of 70–90 ps were achieved [137]. However, the low total number of photons leads to difficulty in estimating the energy deposited in the crystal. Interestingly, the scintillator bismuth germanate (BGO) also provides a good fit for Cerenkov timing. In fact, two recent studies have shown the application of Cerenkov-based timing and scintillation-based energy estimation in BGO crystals, achieving ~200–250 ps with ~ 3 mm long crystals and <330 – 500 ps with 20 mm long crystals coupled to SiPMs [139, 140]. This is important for two reasons: first it moves Cerenkov-based timing with scintillators from a theoretical position to a practical solution, and second because it was done using BGO, a scintillator previously used in commercial PET scanners. Although BGO boasts the highest detection efficiency and photofraction among scintillators used in PET, and is substantially lower in cost than Lu-based scintillators, it became essentially antiquated due to its poor scintillation properties for timing compared to Lu-based scintillators that enabled time-of-flight PET. However, with the prospect of achieving timing resolution with BGO suitable for time-of-flight reconstruction, the revival of BGO for use in high sensitivity, low-cost whole-body systems with at least modest time-of-flight performance now becomes a serious possibility.

The use of prompt Cerenkov photons for timing resolution is currently an active area of research in PET instrumentation, mainly in hopes that it will provide a route to achieve ultimate timing resolution for PET (~ 10 ps) [32, 141]. Right now, one of the major hurdles to overcome is how to efficiently collect the very low number of Cerenkov photons that are produced for a 511 keV photon interaction, typically 10 – 20 in common crystal materials. Therefore, major research directions include optimizing the detector configuration for collecting Cerenkov light, developing an ideal photodetector for detecting the low number of prompt photons, and signal processing methods to make best use of the detected Cerenkov photons. For example, the use of an extremely fast and sensitive photodetector becomes critically important to efficiently use prompt Cerenkov photons for ultimate timing. Further, it has recently been shown that the use of a statistical estimator to estimate timing from multiple time stamps from a prompt timing source leads to larger improvements in timing resolution compared with scintillation-based timing [125], and may be a major enabling component in the effort to achieve a timing resolution of tens of picoseconds.

4.2. Improving spatial resolution

Although recent innovations in spatial resolution for clinical imaging have been relatively modest compared to gains in time-of-flight capabilities, technologically, it is rather simple; superior spatial resolution can be obtained by using smaller scintillator crystals to more accurately determine the photon’s interaction location in the detector. Most clinical scanners make use of detectors that can provide intrinsic spatial resolution of ~ 4 mm and do not have any depth-of-interaction capabilities. However, now with substantially improved time-of-flight capabilities and the trend towards longer axial field-of-view scanners for higher sensitivity, it is very likely that there will be a greater emphasis on improving spatial resolution in clinical scanners. Indeed, some modern systems are now using detectors with ~2.5–3 mm width crystals [28, 84].

However, the use of smaller scintillator crystals in clinical detectors comes with several costs. First is the financial cost associated with manufacturing and fabricating detectors with a large number of small crystals, along with the additional cost due to the increased number of SiPMs needed to read out the smaller crystals. Second is the trade-off between improved spatial resolution with smaller crystals and the associated loss in scintillation light collection, resulting in degraded timing resolution and energy resolution. One promising technology that can create finely pixelated crystal arrays while minimizing light loss and maximizing sensitivity is the use of sub-surface laser engraving or laser induced optical barriers in which a focused high frequency laser is used to create optical boundaries in a large scintillator volume [142–145].

In pre-clinical technology, detector innovations have continued to focus on very small pixelated scintillator arrays coupled to an array of small SiPMs to finely sample the scintillation light [146–152]. These detectors typically use crystals with 0.5 mm – 1 mm width coupled to an array of SiPMs or a similar solid state photodetector, avalanche photodiodes (APDs), leading to spatial resolution as low as ~ 0.5 mm [147]. The main challenges associated with developing high resolution detectors are fabricating finely pixelated crystal arrays (< 1 mm crystal width) with sufficient light output needed to decode all the crystals in the array using SiPMs that are much larger than the crystal width, as it is generally necessary to use SiPMs larger than 1 mm for practical reasons related to cost and read-out electronics.

Monolithic detectors are a promising avenue for realizing superior detector spatial resolution, without the same trade-offs in sensitivity, timing resolution and energy resolution associated with pixelated detectors [72]. For example, recent studies have shown that monolithic detectors using 20 mm thick crystal (suitable for high sensitivity clinical systems) combined with maximum likelihood position estimation or other statistical estimators such as *k*-nearest neighbors can achieve intrinsic spatial resolution of 1.7 mm with single-ended read-out and 1.1 mm with dual-ended read-out, combined with an energy resolution of 10.2% [117]. With thinner scintillators which are acceptable for pre-clinical imaging, spatial resolution of < 1 mm can be achieved [153–155]. One of the potential advantages of this technology for spatial resolution is the ability to set the detector spatial encoding to any arbitrary precision (limited by the intrinsic spatial resolution) since the spatial encoding is not limited by the crystal size as in a pixelated scintillator array. However, the truncation of light transport at the edges of thick monolithic block normally leads to significant non-uniformity in the spatial resolution across the detector, but these losses can be reduced with dual-ended read-out [117]. A further practical challenge with using monolithic detectors in a large system is the complex calibration needed to correlate the measured light distribution to all possible positions of interaction in the detector. In the simplest case, a collimated 511 keV pencil beam is used to irradiate the detector over the entire crystal surface so that the true position of interaction is known and allows mapping measured light distributions to the beam position. This process is relatively straight-forward, albeit time-consuming, in a research lab setting for a small number of detectors, but may become problematic in a large system. However, the development of efficient calibration methods is an active area of research [156, 157], and so we do not expect this to be a major limiting factor preventing the adoption of monolithic detectors.

Alternatively, CZT and TlBr semiconductor detectors have demonstrated excellent spatial resolution (~ 0.5 – 1 mm) [78, 158–162]. The direct detection of annihilation photons with semiconductor detectors overcomes two of the critical limitations associated with very small pixelated scintillator arrays; first the challenges associated with fabricated finely pixelated scintillator arrays, and second the difficulty in efficiently extracting scintillation out of the long narrow crystals.

The main practical challenge associated with semiconductor detectors is the difficulty in growing chemically pure and structurally uniform crystals [163], which limits the achievable thickness of these detectors needed for high sensitivity. Along with this, the timing resolution of semiconductor detectors is very poor compared to scintillators, typically ~10 ns, a result of the relatively slow drift time of charge carriers in the semiconductor material [164], However, a novel solution to significantly enhance the timing resolution of TlBr detectors has recently been proposed and measured based on Cerenkov emissions. Similar to BGO, TlBr is characterized by a very high refractive index (~2.4) and high photofraction, along with a unique semiconductor property in that it is reasonably transparent for visible light due to its large bandgap. These properties suggest the potential for using Cerenkov photons for fast timing resolution. The feasibility of enabling time-of-flight capabilities in a TlBr was recently demonstrated in a proof-of-concept study, showing timing resolution of 430 ps could be achieved with SiPM read-out of Cerenkov light [165]. Combining the readout of Cerenkov light using SiPMs with charge readout from the semiconductor for position and energy estimation remains to be implemented, but this is a highly promising method to combine the attractive energy resolution and stopping power of TlBr with fast timing resolution for time-of-flight applications.

4.2.1. Depth of interaction—One of the major research topics in PET detector instrumentation that accompanies high resolution scanners is the development of depth-of-interaction (DOI) encoding detectors [38] (Figure 4). When a 511 keV enters the detector at an oblique angle, the variable depth in the scintillator at which the photon can be absorbed introduces blurring in the spatial point spread function. In clinical whole-body scanners with a narrow axial field-of-view, DOI effects introduce only minor radial blurring, but becomes a limiting factor for spatial resolution in smaller bore scanners, such as pre-clinical and dedicated organ scanners. However, there is now interest in developing DOI encoding technology with time-of-flight capabilities, either for ultrahigh performance brain imaging systems, or for long axial field-of-view whole-body systems where there is axial blurring associated with a wide axial acceptance angle [166]. This task is poses challenges to minimize the trade-offs between DOI encoding, energy resolution and timing resolution, since most DOI encoding strategies often result in considerable loss of scintillation light leading to poor energy resolution and timing resolution, an acceptable trade-off for preclinical imaging, but unacceptable in clinical imaging systems.

One of the highest performance DOI encoding strategies is to place photodetectors at the front and back of the scintillator crystal array in the so-called dual-ended configuration, and DOI resolution as good as 2 mm have been achieved [167–169]. In this configuration, the depth of interaction of the annihilation photon in the crystal will influence how much scintillation light reaches each end of the scintillator array, and therefore measuring these

differences with photodetectors at the front and back of the array can be used to estimate DOI. With appropriate scintillator array design (i.e. reflector and surface finish) for efficient light collection, dual-ended DOI detectors can also provide excellent timing resolution [115, 116]. Of course, the main downside of these detectors is the requirement for double the number of photodetectors and electronic channels (increasing both cost and system complexity), as well as the mechanical difficulty in constructing detector rings with photodetectors inside the scanner bore, mainly in terms of achieving compact assembly and integrating cooling.

In monolithic detectors, DOI information is intrinsically present in the distribution of scintillation light on the photodetectors [170–172]. For instance, if the 511 keV is absorbed near the front of the scintillator (i.e. away from the photodetectors coupled to the backside of the crystal), the light distribution will be more broad than if the photon is absorbed near the back of the scintillator. In this configuration, DOI resolution of 3–5 mm has been measured with 22 mm thick LYSO scintillator [173]. However, when combining monolithic detectors with dual-ended readout DOI resolution improved to 2.5 mm [117]. Therefore, this detector appears a very promising candidate to provide excellent 3D positioning accuracy, excellent energy resolution, and exceptional time-of-flight performance.

Another common DOI encoding scheme is to stack layers of scintillators. The scintillator layers can vary in their temporal emission properties such as decay time [33, 174], or can be configured such that interactions in each layer produces a unique spatial distribution of scintillation light incident on the photodetectors [143, 175–177]. However, one of the major limitations for these methods is the loss of scintillation light at each crystal interface resulting in generally poor timing resolution and energy resolution, however this can be minimized with novel fabrication techniques [178–181].

Lastly, DOI information can be obtained by applying a thin layer of phosphor to the sides of scintillator crystals [182]. The phosphor coating absorbs a fraction of the scintillation light and introduces DOI-dependent changes in the temporal properties of the scintillation light. One of the important recent developments in this detector has been the development of maximum likelihood pulse shape discrimination methods to better extract the DOI from the photodetector waveforms, resulting in DOI positioning accuracy of < 2 mm in single crystals [183]. In addition, although the phosphor coating the feasibility of phosphor-coated crystals for combined DOI and time-of-flight application has been demonstrated [184–186].

4.3. Improving energy resolution

Detectors used in modern clinical scanners employing LSO/LYSO coupled to SiPMs generally provide energy resolution of 10–12% at 511 keV, compared to ~ 15–20% for high resolution detectors used in pre-clinical systems. For pre-clinical imaging, there is comparatively low demand on achieving optimal energy resolution given the low scatter fraction in the small animals, and so energy resolution is usually traded off for higher spatial resolution using finely pixelated scintillator arrays that reduces the overall light output.

With common scintillation-based detectors, energy resolution is dominated by statistical variance arising from the relatively low number of generated and collected scintillation

photons, and the non-proportionality of the scintillator light output, leading to energy resolutions of ~10–12% [187]. The high PDE of SiPMs has enabled small improvements in energy resolution with LSO/LYSO, but the relatively low number of scintillation photons and non-proportionality of most Lu scintillators continues to limit energy resolution. Therefore, one of the most obvious routes to improve energy resolution is the use of brighter scintillators. For example, garnet scintillators (GAGG, GGAG, and GluGAGG) can provide substantially better energy resolution than LYSO (~7–8%) owing to their high light output [188, 189]. The halide scintillators, $CeBr_3$ and $LaBr_3$, provide ~2-fold higher light output compared to LSO/LYSO, leading to energy resolutions of < 7% [108, 190, 191], and recently values as good as ~ 2–3% have been achieved when combined with Sr co-doping to further increase light output and reduce non-proportionality [192, 193].

One of the critical limitations regarding energy resolution with LSO/LYSO scintillators is their non-proportionality. Here, non-proportionality refers to the non-linear scintillation light output in relation to the energy deposited by the interacting photon. Lu-based scintillators typically exhibit decreasing proportionality of light output as the deposited energy decreases. This non-proportionality results in large differences in overall light output depending on how the 511 keV is absorbed in the scintillator (i.e. a single photoelectric absorption vs. multiple Compton interactions followed by photoelectric absorption), and is the main reason why common Lu-based scintillators such as LYSO/LSO cannot currently achieve their predicted intrinsic energy resolution of <6% based only on the statistical uncertainty in the number of generated photons. Some Lu-based scintillators have been developed with superior proportionality, including LuAP and LuYAP [187]. Although the light outputs of these scintillators are less than that of L(Y)SO suggesting poorer energy resolution due to the statistical randomness, they achieve similar energy resolution as a result of the lower non-proportionality. The further benefit of LuAP is its higher density and short decay time.

The solution for ultimate energy resolution likely resides in the use of direct semiconductor detectors. The absorption of a 511 keV photon in a semiconductor, such as CZT or TlBr, produces several orders of magnitude more charge carriers than the number of photons in scintillators, resulting in lower statistical variance and therefore superior energy resolution, as good as ~2–3% in several studies [194–197].

5. Future PET scanners

The sustained improvements in time-of-flight performance will likely continue to provide some of the most significant advances in PET technology for clinical imaging. Time-of-flight performance of commercially available scanners has improved substantially in the past two years, with several manufacturers now boasting timing resolutions of 300 – 350 ps [70, 84, 85], nearly a two-fold improvement from five years prior, along with prototype systems with ~ 100 ps timing resolution [110]. It is unlikely that next generation time-of-flight scanners will deviate from using Lu-based scintillators in the near future, due to their excellent scintillation properties and their availability through high-quality mass production, although further refinements in the crystal properties, such as through co-doping, may be possible. In general, we foresee that developments in SiPM technology that provide higher PDE, lower noise, and lower timing jitter, coupled with advanced electronics and signal

processing methods will continue to push the boundary of achievable timing resolution, resulting in scanners with < 200 ps timing resolution becoming commonplace. It remains to be seen whether this standard detector technology (LYSO + SiPMs) will be capable of achieving the next milestone in time-of-flight performance in a PET system, namely sub-100ps timing resolution. It is likely that a combination of new scintillator technology, significant improvements in the time response of SiPMs, advanced signal processing methods, or a new timing mechanism such as Cerenkov based timing, are needed to realize this time-of-flight capability in whole-body systems.

The second major expected innovation in PET technology is optimized system geometries for high sensitivity whole-body imaging and dedicated organ imaging. With two systems currently under development at UC Davis and the University of Pennsylvania, along with promising initial preclinical results in non-human primates with a smaller-scale long axial field-of-view scanner [198], it is reasonable to expect this technology to be introduced in the clinic in some capacity. In the first realizations, the main emphasis of these scanners will be to maximize geometric sensitivity, using relatively commonplace detector technology, characterized by ~ 300 – 400 ps timing resolution, ~ 3 mm spatial resolution and ~ 10–12% energy resolution. The optimal scanner length remains to be determined, and will be driven by several factors, primarily cost and the use and benefit of such scanners for clinical and research applications, some of which are known (e.g. shorter scan time, improved lesion detection) as well as unknown applications that have yet to be realized with PET.

For dedicated brain scanners, optimized system geometries to maximize scanner sensitivity, high spatial resolution detectors providing ~1–2 mm spatial resolution with depth-encoding, as well as the possibility of further image quality improvement with < 200 ps time-of-flight, are likely to be developed. It does not seem unreasonable to anticipate high-sensitivity brain scanners that achieve <2 mm spatial resolution, made possible by the use of high resolution pixelated detectors or monolithic detectors with DOI capabilities. Additionally, these scanners should make use of continual improvements in time-of-flight capabilities once the practically achievable timing resolution reaches ~150 ps.

It seems likely that monolithic detectors may be instrumental in realizing higher performance in future PET systems. Monolithic detectors have the ability to provide high intrinsic detection sensitivity due to the absence of gaps between crystals that is present in conventional pixelated detectors, and also provide excellent energy resolution and time-of-flight performance due to the efficient light transport in the large crystal block, and excellent spatial resolution including DOI encoding that will likely become increasingly important as scanner sensitivity and time-of-flight performance increases. Additionally, the use of statistical estimators, such as maximum likelihood, can simultaneously make use of both the spatial and temporal information contained in the detected scintillation light for optimal performance. Therefore, we see the possibility for this detector technology to play a central role in future high-performance PET systems for several applications, including whole-body time-of-flight scanners with extended axial field-of-view, and dedicated brain scanners. The largest challenges in implementing these detectors is to minimize the loss of spatial resolution at the detector edges which are typically substantial for thick monolithic

scintillators, and develop practical calibration schemes for large scale PET systems that incorporate these detectors.

Looking farther in the future, we envision a high-performance scanner, with long axial field-of-view of >1 meter making use of monolithic detectors with the ability to digitize and store waveforms from individual photodetectors for application of maximum likelihood or machine learning signal processing, all combined to provide maximal geometric scanner sensitivity, ~ 150 ps time-of-flight, and ~2 mm spatial resolution. Although such a scanner is at least several years in the future, most of the necessary components are reasonably mature at least in laboratory bench-settings, and so we do not think such a scanner to be merely a fancy thought experiment. There also will be strong pressures and efforts to reduce cost while maintaining performance which will drive development of new detector materials, the area where cost-savings are likely most easily realized.

Naturally, future PET systems will also continue to be integrated with state-of-the-art CT and MRI systems, where impressive technological development also continues to occur. For example, photon-counting x-ray detectors [199] are one obvious area with the potential to reduce dose and/or improve image quality in CT. We also must impress on the reader that in parallel to the advances in PET scanner and detector technology outlined in this article, there are equally important and significant developments in data corrections, processing, image reconstruction and kinetic modeling that have not been discussed here, but continue to advance and provide significant contributions to the capabilities of PET imaging. Examples include 4D reconstruction that incorporates information in the temporal domain, exploiting time-of-flight information to aid in a range of data corrections and improve the robustness of quantitative measurements and joint reconstructions using other imaging data. Combining these emerging technological and methodological advances promises to lead to a generation of PET scanners tailored for specific applications that really can claim to approach the fundamental limits set forth by the physics of radioactive decay and the statistics of the available signal.

Acknowledgments

The authors gratefully acknowledge the many discussions and insights from colleagues and collaborators at UC Davis and around the world for shaping the thoughts that form the basis for this review. Our contribution is dedicated to the memory of Dr. Christopher J. Thompson (1942–2017), a pioneer in PET instrumentation who made important and sustained contributions to our field for over forty years, not only for his many scientific achievements, but also for the impeccable way in which he represented his profession and for his generous spirit.

References

1. Jones T, Townsend D. History and future technical innovation in positron emission tomography. J Med Imaging. 2017; 4:011013.
2. Muehllehner G, Karp JS. Positron emission tomography. Phys Med Biol. 2006; 51:R117–R137. [PubMed: 16790899]
3. Vallabhajosula S, Solnes L, Vallabhajosula B. A broad overview of positron emission tomography radiopharmaceuticals and clinical applications: What is new? Semin Nucl Med. 2011; 41:246–264. [PubMed: 21624560]
4. Carson, RE. Tracer kinetic modeling in PET. In: Bailey, DL.Townsend, DW.Valk, PE., Maisey, MN., editors. Positron Emission Tomography: Basic Sciences. London: Springer; 2005. p. 127-159.

5. Wrenn FR, Good ML, Handler P. The use of positron-emitting radioisotopes for the localization of brain tumors. Science. 1951; 113:525–527. [PubMed: 14828392]
6. Brownell GL, Sweet WH. Localization of brain tumors with positron emitters. Nucleonics. 1953; 11:40–45.
7. Phelps ME, Hoffman EJ, Mullani NA, et al. Application of annihilation coincidence detection to transaxial reconstruction tomography. J Nucl Med. 1975; 16:210–224. [PubMed: 1113170]
8. Ter-Pogossian MM, Phelps ME, Hoffman EJ, et al. A positron-emission transaxial tomograph for nuclear imaging (PETT). Radiology. 1975; 114:89–98. [PubMed: 1208874]
9. Rowland DJ, Cherry SR. Small-animal preclinical nuclear medicine instrumentation and methodology. Semin Nucl Med. 2008; 38:209–222. [PubMed: 18396180]
10. Townsend DW. Positron emission tomography/computed tomography. Semin Nucl Med. 2008; 38:152–166. [PubMed: 18396176]
11. Vandenberghe S, Marsden PK. PET-MRI: a review of challenges and solutions in the development of integrated multimodality imaging. Phys Med Biol. 2015; 60:R115–R154. [PubMed: 25650582]
12. Townsend DW. Multimodality imaging of structure and function. Phys Med Biol. 2008; 53:R1–R39. [PubMed: 18263942]
13. Cherry, SR., Sorenson, JA., Phelps, NE. Physics in Nuclear Medicine. Saunders; 2012.
14. Surti S. Update on time-of-flight PET imaging. J Nucl Med. 2015; 56:98–105. [PubMed: 25525181]
15. Tong S, Alessio AM, Kinahan PE. Image reconstruction for PET/CT scanners: Past achievements and future challenges. Imag Med. 2010; 2:529–545.
16. Author. Performance Measurements of Positron Emission Tomographs (PETs): NU2-2012. Rosslyn, VA: National Electrical Manufacturers Association; 2013.
17. Hsu DFC, Ilan E, Peterson WT, et al. Studies of a next-generation silicon-photomultiplier-based time-of-flight PET/CT system. J Nucl Med. 2017; 58:1511–1518. [PubMed: 28450566]
18. Vandenberghe S, Mikhaylova E, D'Hoe E, et al. Recent developments in time-of-flight PET. EJNMMI Phys. 2016; 3:3. [PubMed: 26879863]
19. Tomitani T. Image reconstruction and noise evaluation in photon time-of-flight assisted positron emission tomography. IEEE Trans Nucl Sci. 1981; 28:4581–4589.
20. Snyder DL, Thomas LJ, Ter-Pogossian MM. A mathematical model for positron-emission tomography systems having time-of-flight measurements. IEEE Trans Nucl Sci. 1981; 28:3575–3583.
21. Cherry SR. The 2006 Henry N. Wagner Lecture: Of mice and men (and positrons)— advances in PET imaging technology. J Nucl Med. 2006; 47:1735–1745. [PubMed: 17079804]
22. Judenhofer MS, Cherry SR. Applications for preclinical PET/MRI. Semin Nucl Med. 2013; 43:19–29. [PubMed: 23178086]
23. Tsoumpas C, Visvikis D, Loudos G. Innovations in small-animal PET/MR imaging instrumentation. PET Clinics. 2016; 11:105–118. [PubMed: 26952725]
24. Poon JK, Dahlbom ML, Moses WW, et al. Optimal whole-body PET scanner configurations for different volumes of LSO scintillator: a simulation study. Phys Med Biol. 2012; 57:4077–4094. [PubMed: 22678106]
25. Poon, JK. Ph D Thesis. University of California; Davis: 2013. The performance limits of long axial field of view PET scanners.
26. Zhang XZ, Zhou J, Cherry SR, et al. Quantitative image reconstruction for total-body PET imaging using the 2-meter long EXPLORER scanner. Phys Med Biol. 2017; 62:2465–2485. [PubMed: 28240215]
27. Cherry SR, Badawi RD, Karp JS, et al. Total-body imaging: Transforming the role of positron emission tomography. Sci Transl Med. 2017; 9:eaaf6169. [PubMed: 28298419]
28. Cherry SR, Jones T, Karp JS, et al. Total-body PET: Maximizing sensitivity to create new opportunities for clinical research and patient care. J Nucl Med. 2018; 59:3–12. [PubMed: 28935835]
29. Schmall J, Karp JS, Werner M, et al. Parallax error in long-axial field-of-view PET scanners—a simulation study. Phys Med Biol. 2016; 61:5443–5455. [PubMed: 27367971]

30. Surti S, Karp JS. Impact of detector design on imaging performance of a long axial field-of-view, whole-body PET scanner. Phys Med Biol. 2015; 60:5343–58. [PubMed: 26108352]
31. Mikhaylova E, Tabacchini V, Borghi G, et al. Optimization of an ultralow-dose high-resolution pediatric PET scanner design based on monolithic scintillators with dual-sided digital SiPM readout: a simulation study. Phys Med Biol. 2017; 62:8402–8418. [PubMed: 28944759]
32. Lecoq P. Pushing the limits in time-of-flight PET imaging. IEEE Trans Radiat Plasma Med Sci. 2017; 1:473–485.
33. de Jong HW, van Velden FH, Kloet RW, et al. Performance evaluation of the ECAT HRRT: An LSO-LYSO double layer high resolution, high sensitivity scanner. Phys Med Biol. 2007; 52:1505–26. [PubMed: 17301468]
34. Kolb A, Wehrl HF, Hofmann M, et al. Technical performance evaluation of a human brain PET/MRI system. Eur Radiol. 2012; 22:1776–1788. [PubMed: 22752524]
35. Watanabe M, Saito A, Isobe T, et al. Performance evaluation of a high-resolution brain PET scanner using four-layer MPPC DOI detectors. Phys Med Biol. 2017; 62:7148–7166. [PubMed: 28753133]
36. Gong K, Majewski S, Kinahan PE, et al. Designing a compact high performance brain PET scanner—simulation study. Phys Med Biol. 2016; 61:3681–97. [PubMed: 27081753]
37. Tashima H, Yamaya T. Proposed helmet PET geometries with add-on detectors for high sensitivity brain imaging. Phys Med Biol. 2016; 61:7205–7220. [PubMed: 27649355]
38. Ito M, Hong SJ, Lee JS. Positron emission tomography (PET) detectors with depth-of-interaction (DOI) capability. Biomed Eng Lett. 2011; 1:70.
39. Bauer CE, Brefczynski-Lewis J, Marano G, et al. Concept of an upright wearable positron emission tomography imager in humans. Brain and Behavior. 2016; 6:e00530. [PubMed: 27688946]
40. Berg WA. Nuclear breast imaging: Clinical results and future directions. J Nucl Med. 2016; 57:46S–52S. [PubMed: 26834102]
41. Hsu DFC, Freese DL, Levin CS. Breast-dedicated radionuclide imaging systems. J Nucl Med. 2016; 57:40S–45S. [PubMed: 26834101]
42. MacDonald L, Edwards J, Lewellen T, et al. Clinical imaging characteristics of the positron emission mammography camera: PEM Flex Solo II. J Nucl Med. 2009; 50:1666–1675. [PubMed: 19759118]
43. Raylman RR, Majewski S, Smith MF, et al. The positron emission mammography/tomography breast imaging and biopsy system (PEM/PET): design, construction and phantom-based measurements. Phys Med Biol. 2008; 53:637–53. [PubMed: 18199907]
44. Abreu MC, Aguiar JD, Almeida FG, et al. Design and evaluation of the clear-PEM scanner for positron emission mammography. IEEE Trans Nucl Sci. 2006; 53:71–77.
45. Iima M, Nakamoto Y, Kanao S, et al. Clinical performance of 2 dedicated PET scanners for breast imaging: Initial evaluation. J Nucl Med. 2012; 53:1534–1542. [PubMed: 22933819]
46. Miyake KK, Matsumoto K, Inoue M, et al. Performance evaluation of a new dedicated breast PET scanner using NEMA NU4-2008 standards. J Nucl Med. 2014; 55:1198–1203. [PubMed: 24812244]
47. Moliner L, González AJ, Soriano A, et al. Design and evaluation of the MAMMI dedicated breast PET. Med Phys. 2012; 39:5393–5404. [PubMed: 22957607]
48. Bowen SL, Wu Y, Chaudhari AJ, et al. Initial characterization of a dedicated breast PET/CT scanner during human imaging. J Nucl Med. 2009; 50:1401–1408. [PubMed: 19690029]
49. Larobina M, Brunetti A, Salvatore M. Small animal PET: A review of commercially available imaging systems. Curr Med Imag Rev. 2006; 2:187–192.
50. Vaska P, Cao TY. The state of instrumentation for combined positron emission tomography and magnetic resonance imaging. Semin Nucl Med. 2013; 43:11–18. [PubMed: 23178085]
51. Yang Y, Bec J, Zhou J, et al. A prototype high-resolution small-animal PET scanner dedicated to mouse brain imaging. J Nucl Med. 2016; 57:1130–1135. [PubMed: 27013696]

52. Espana S, Marcinkowski R, Keereman V, et al. DigiPET: Sub-millimeter spatial resolution small-animal PET imaging using thin monolithic scintillators. Phys Med Biol. 2014; 59:3405–20. [PubMed: 24888974]
53. Schulz D, Southekal S, Junnarkar SS, et al. Simultaneous assessment of rodent behavior and neurochemistry using a miniature positron emission tomograph. Nature Methods. 2011; 8:347–52. [PubMed: 21399637]
54. Kyme A, Se S, Meikle S, et al. Markerless motion tracking of awake animals in positron emission tomography. IEEE Trans Med Imaging. 2014; 33:2180–90. [PubMed: 24988591]
55. Lewellen TK. Recent developments in PET detector technology. Phys Med Biol. 2008; 53:R287–317. [PubMed: 18695301]
56. Parodi K. Vision 20/20: Positron emission tomography in radiation therapy planning, delivery, and monitoring. Med Phys. 2015; 42:7153–7168. [PubMed: 26632070]
57. Nishio T, Miyatake A, Ogino T, et al. The development and clinical use of a beam on-line PET system mounted on a rotating gantry port in proton therapy. Int J Rad Onc Biol Physics. 2010; 76:277–286.
58. Crespo P, Shakirin G, Fiedler F, et al. Direct time-of-flight for quantitative, real-time in-beam PET: A concept and feasibility study. Phys Med Biol. 2007; 52:6795–811. [PubMed: 18029976]
59. Sportelli G, Belcari N, Camarlinghi N, et al. First full-beam PET acquisitions in proton therapy with a modular dual-head dedicated system. Phys Med Biol. 2014; 59:43–60. [PubMed: 24321855]
60. Shao Y, Sun X, Lou K, et al. In-beam PET imaging for on-line adaptive proton therapy: an initial phantom study. Phys Med Biol. 2014; 59:3373–88. [PubMed: 24874943]
61. Maurer T, Eiber M, Schwaiger M, et al. Current use of PSMA-PET in prostate cancer management. Nat Rev Urol. 2016; 13:226–235. [PubMed: 26902337]
62. Huber JS, Choong WS, Moses WW, et al. Characterization of a PET camera optimized for prostate imaging. IEEE Nuclear Science Symposium Conference Record. 2005; 1559:2005.
63. Musico P. The endo-rectal probe prototype for the TOPEM project. Nucl Inst Meth A. 2016; 824:218–219.
64. Mathews AJ, Komarov S, Wu H, et al. Improving PET imaging for breast cancer using virtual pinhole PET half-ring insert. Phys Med Biol. 2013; 58:6407–27. [PubMed: 23999026]
65. Lee S, Kross B, McKisson J, et al. Imaging corn plants with PhytoPET, a modular PET system for plant biology. 2013 IEEE Nuclear Science Symposium and Medical Imaging Conference (2013 NSS/MIC). 2013
66. Beer S, Streun M, Hombach T, et al. Design and initial performance of PlanTIS: A high-resolution positron emission tomograph for plants. Phys Med Biol. 2010; 55:635–46. [PubMed: 20071758]
67. Wang Q, Mathews AJ, Li K, et al. A dedicated high-resolution PET imager for plant sciences. Phys Med Biol. 2014; 59:5613–29. [PubMed: 25190198]
68. Casey M, Nutt R. A multicrystal two dimensional BGO detector system for positron emission tomography. IEEE Trans Nucl Sci. 1986; 1:460–463.
69. Ota R, Omura T, Yamada R, et al. Evaluation of a sub-millimeter resolution pet detector with a 1.2 mm pitch TSV-MPPC array one-to-one coupled to LFS scintillator crystals and inter-crystal scatter studies with individual signal readout. IEEE Trans Rad Plasma Med Sci. 2017; 1:15–22.
70. Miller M, Zhang J, Binzel K, et al. Characterization of the Vereos digital photon counting PET system. J Nucl Med. 2015; 56(suppl):434.
71. Schaart DR, van Dam HT, Seifert S, et al. A novel, SiPM-array-based, monolithic scintillator detector for PET. Phys Med Biol. 2009; 54:3501–12. [PubMed: 19443953]
72. Joung J, Miyaoka RS, Lewellen TK. cMiCE: A high resolution animal PET using continuous LSO with a statistics based positioning scheme. Nucl Inst Meth A. 2002; 489:584–598.
73. Melcher C, Schweitzer J. Cerium-doped lutetium oxyorthosilicate: a fast, efficient new scintillator. IEEE Trans Nucl Sci. 1992; 39:502–505.
74. Roncali E, Cherry SR. Application of silicon photomultipliers to positron emission tomography. Ann Biomed Eng. 2011; 39:1358–1377. [PubMed: 21321792]
75. Renker D. New trends on photodetectors. Nucl Inst Meth A. 2007; 571:1–6.

76. Schaart DR, Charbon E, Frach T, et al. Advances in digital SiPMs and their application in biomedical imaging. Nucl Inst Meth A. 2016; 809:31–52.
77. Frach T, Prescher G, Degenhardt C, et al. The digital silicon photomultiplier—Principle of operation and intrinsic detector performance. 2009 IEEE Nuclear Science Symposium Conference Record (NSS/MIC). 2009:1959–1965.
78. Del Sordo S, Abbene L, Caroli E, et al. Progress in the development of CdTe and CdZnTe semiconductor radiation detectors for astrophysical and medical applications. Sensors. 2009; 9:3491–3526. [PubMed: 22412323]
79. Vandenberghe S, Mikhaylova E, D'Hoe E, et al. Recent developments in time-of-flight PET. Eur J Nucl Med Mol Imaging. 2016; 3:1.
80. Surti S, Karp JS. Advances in time-of-flight PET. Physica Medica. 2016; 32:12–22. [PubMed: 26778577]
81. Jakoby BW, Bercier Y, Conti M, et al. Physical and clinical performance of the mCT time-of-flight PET/CT scanner. Phys Med Biol. 2011; 56:2375–89. [PubMed: 21427485]
82. Zaidi H, Ojha N, Morich M, et al. Design and performance evaluation of a whole-body Ingenuity TF PET–MRI system. Phys Med Biol. 2011; 56:3091. [PubMed: 21508443]
83. Bettinardi V, Presotto L, Rapisarda E, et al. Physical performance of the new hybrid PET/CT Discovery-690. Med Phys. 2011; 38:5394–5411. [PubMed: 21992359]
84. Casey M, Burbar Z, Rothfuss H, et al. A next generation SiPM based PET/CT system with improved time and spatial resolution. J Nucl Med. 2017; 58:1332–1332.
85. Hsu DF, Ilan E, Peterson WT, et al. Studies of a next generation silicon-photomultiplier-based time-of-flight PET/CT system. J Nucl Med. 2017:1511–1518. [PubMed: 28450566]
86. Levin CS, Maramraju SH, Khalighi MM, et al. Design features and mutual compatibility studies of the time-of-flight PET capable GE SIGNA PET/MR System. IEEE Trans Med Imaging. 2016; 35:1907–14. [PubMed: 26978664]
87. Cates JW, Levin CS. Advances in coincidence time resolution for PET. Phys Med Biol. 2016; 61:2255–64. [PubMed: 26914187]
88. Gundacker S, Acerbi F, Auffray E, et al. State of the art timing in TOF-PET detectors with LuAG, GAGG and L(Y)SO scintillators of various sizes coupled to FBK-SiPMs. J Instr. 2016; 11:08008.
89. Nemallapudi MV, Gundacker S, Lecoq P, et al. Sub-100 ps coincidence time resolution for positron emission tomography with LSO:Ce codoped with Ca. Phys Med Biol. 2015; 60:4635–49. [PubMed: 26020610]
90. Bisogni MG, Morrocchi M. Development of analog solid-state photo-detectors for positron emission tomography. Nucl Inst Meth A. 2016; 809:140–148.
91. Yamamoto K, Sato K, Yamada R, et al. Assembly technology of 4-side buttable MPPC. Nucl Inst Meth A. 2013; 732:547–550.
92. Goertzen AL, Stortz G, Thiessen JD, et al. First results from a high-resolution small animal SiPM PET insert for PET/MR imaging at 7T. IEEE Trans Nucl Sci. 2016; 63:2424–2433.
93. Ko GB, Yoon HS, Kim KY, et al. Simultaneous multiparametric PET/MRI with silicon photomultiplier PET and ultra-high-field MRI for small-animal imaging. J Nucl Med. 2016; 57:1309–1315. [PubMed: 27081173]
94. Schug D, Lerche C, Weissler B, et al. Initial PET performance evaluation of a preclinical insert for PET/MRI with digital SiPM technology. Phys Med Biol. 2016; 61:2851–78. [PubMed: 26987774]
95. Spurrier MA, Szupryczynski P, Yang K, et al. Effects of co-doping on the scintillation properties of LSO:Ce. IEEE Trans Nucl Sci. 2008; 55:1178–1182.
96. Gundacker S, Auffray E, Pauwels K, et al. Measurement of intrinsic rise times for various L(Y)SO and LuAG scintillators with a general study of prompt photons to achieve 10 ps in TOF-PET. Phys Med Biol. 2016; 61:2802–37. [PubMed: 26982798]
97. Doroud K, Williams M, Zichichi A, et al. Comparative timing measurements of LYSO and LFS-3 to achieve the best time resolution for TOF-PET. Nucl Inst Meth A. 2015; 793:57–61.
98. Yamamoto S, Okumura S, Kato N, et al. Timing measurements of lutetium based scintillators combined with silicon photomultipliers for TOF-PET system. J Instr. 2015; 10:T09002.

99. Wang Y, Baldoni G, Rhodes WH, et al. Transparent garnet ceramic scintillators for gamma-ray detection. Proc SPIE. 2012; 850717
100. Kamada, K., Yanagida, T., Endo, T., et al. Nuclear Science Symposium and Medical Imaging Conference (NSS/MIC), 2011. IEEE; 2011. 2-inch size single crystal growth and scintillation properties of new scintillator; Ce:$Gd_3Al_2Ga_3O_{12}$; p. 1927-1929.
101. Lucchini M, Babin V, Bohacek P, et al. Effect of Mg^{2+} ions co-doping on timing performance and radiation tolerance of Cerium doped $Gd_3Al_2Ga_3O_{12}$ crystals. Nucl Inst Meth A. 2016; 816:176–183.
102. Schneider FR, Shimazoe K, Somlai-Schweiger I, et al. A PET detector prototype based on digital SiPMs and GAGG scintillators. Phys Med Biol. 2015; 60:1667–79. [PubMed: 25633017]
103. Yanagida T, Fujimoto Y, Yagi H, et al. Optical and scintillation properties of transparent ceramic Yb:Lu_2O_3 with different Yb concentrations. Optical Materials. 2014; 36:1044–1048.
104. Fukabori A, Chani V, Kamada K, et al. Growth of Yb-doped Y_2O_3, Sc_2O_3, and Lu_2O_3 single crystals by the micro-pulling-down technique and their optical and scintillation characterization. J Crystal Growth. 2012; 352:124–128.
105. Shah KS, Glodo J, Higgins W, et al. $CeBr_3$ scintillators for gamma-ray spectroscopy. Nuclear Science Symposium Conference Record, 2004 IEEE. 2004:4278–4281.
106. Surti S, Karp J, Muehllehner G, et al. Investigation of lanthanum scintillators for 3D PET. Nuclear Science Symposium Conference Record, 2002 IEEE. 2002:1177–1181.
107. Schaart DR, Seifert S, Vinke R, et al. $LaBr_3$: Ce and SiPMs for time-of-flight PET: achieving 100 ps coincidence resolving time. Phys Med Biol. 2010; 55:N179–89. [PubMed: 20299734]
108. Kuhn A, Surti S, Karp J, et al. Design of a lanthanum bromide detector for time-of-flight PET. IEEE Trans Nucl Sci. 2004; 51:2550–2557.
109. Glodo J, Moses W, Higgins W, et al. Effects of Ce concentration on scintillation properties of $LaBr_3$:Ce. IEEE Trans Nucl Sci. 2005; 52:1805–1808.
110. Peng Q, Moses W, Zhang X, et al. Development of tachyon time-of-flight PET cameras. Nuclear Science Symposium, Medical Imaging Conference and Room-Temperature Semiconductor Detector Workshop (NSS/MIC/RTSD), 2016. 2016
111. Daube-Witherspoon M, Surti S, Perkins A, et al. The imaging performance of a $LaBr_3$-based PET scanner. Phys Med Biol. 2009; 55:45–64.
112. Gundacker S, Knapitsch A, Auffray E, et al. Time resolution deterioration with increasing crystal length in a TOF-PET system. Nucl Inst Meth A. 2014; 737:92–100.
113. Spanoudaki VC, Levin C. Investigating the temporal resolution limits of scintillation detection from pixellated elements: comparison between experiment and simulation. Phys Med Biol. 2011; 56:735–56. [PubMed: 21239845]
114. Lecoq P, Auffray E, Knapitsch A. How photonic crystals can improve the timing resolution of scintillators. IEEE Trans Nucl Sci. 2013; 60:1653–1657.
115. Derenzo SE, Choong W-S, Moses WW. Monte Carlo calculations of PET coincidence timing: single and double-ended readout. Phys Med Biol. 2015; 60:7309–38. [PubMed: 26350162]
116. Seifert S, Schaart DR. Improving the time resolution of TOF-PET detectors by double-sided readout. IEEE Trans Nucl Sci. 2015; 62:3–11.
117. Borghi G, Peet BJ, Tabacchini V, et al. A 32 mm× 32 mm× 22 mm monolithic LYSO:Ce detector with dual-sided digital photon counter readout for ultrahigh-performance TOF-PET and TOF-PET/MRI. Phys Med Biol. 2016; 61:4929–49. [PubMed: 27286232]
118. Spanoudaki V, Levin CS. Photo-detectors for time of flight positron emission tomography (ToF-PET). Sensors. 2010; 10:10484–505. [PubMed: 22163482]
119. Acerbi F, Ferri A, Zappala G, et al. NUV silicon photomultipliers with high detection efficiency and reduced delayed correlated-noise. IEEE Trans Nucl Sci. 2015; 62:1318–1325.
120. Piemonte C, Acerbi F, Ferri A, et al. Performance of NUV-HD silicon photomultiplier technology. IEEE Trans Elec Dev. 2016; 63:1111–1116.
121. Gola A, Ferri A, Tarolli A, et al. SiPM optical crosstalk amplification due to scintillator crystal: effects on timing performance. Phys Med Biol. 2014; 59:3615–35. [PubMed: 24922188]

122. Acerbi F, Ferri A, Gola A, et al. Analysis of single-photon time resolution of FBK silicon photomultipliers. Nucl Instr Meth A. 2015; 787:34–37.
123. Nemallapudi M, Gundacker S, Lecoq P, et al. Single photon time resolution of state of the art SiPMs. J Instr. 2016; 11:10016.
124. Nolet F, Dubois F, Roy N, et al. Digital SiPM channel integrated in CMOS 65 nm with 17.5 ps FWHM single photon timing resolution. Nucl Inst Meth A. 2017
125. Tétrault M-A, Therrien AC, Lemaire W, et al. TDC array tradeoffs in current and upcoming digital SiPM detectors for time-of-flight PET. IEEE Trans Nucl Sci. 2017; 64:925–932.
126. Gros-Daillon E, Maingault L, André L, et al. First characterization of the SPADnet sensor: a digital silicon photomultiplier for PET applications. J Instr. 2013; 8:C12026.
127. Gundacker S, Auffray E, Jarron P, et al. On the comparison of analog and digital SiPM readout in terms of expected timing performance. Nucl Inst Meth A. 2015; 787:6–11.
128. Anghinolfi F, Jarron P, Martemiyanov A, et al. NINO: an ultra-fast and low-power front-end amplifier/discriminator ASIC designed for the multigap resistive plate chamber. Nucl Instr Meth A. 2004; 533:183–187.
129. Matsuda H, Kataoka J, Ikeda H, et al. Development of ultra-fast ASIC for future PET scanners using TOF-capable MPPC detectors. Nucl Inst Meth A. 2013; 699:211–215.
130. Rolo M, Bugalho R, Goncalves F, et al. TOFPET ASIC for PET applications. J Instr. 2013; 8:C02050.
131. Yeom JY, Vinke R, Levin CS. Optimizing timing performance of silicon photomultiplier-based scintillation detectors. Phys Med Biol. 2013; 58:1207–20. [PubMed: 23369872]
132. van Dam HT, Borghi G, Seifert S, et al. Sub-200 ps CRT in monolithic scintillator PET detectors using digital SiPM arrays and maximum likelihood interaction time estimation. Phys Med Biol. 2013; 58:3243–57. [PubMed: 23611889]
133. Venialgo E, Mandai S, Gong T, et al. Time estimation with multichannel digital silicon photomultipliers. Phys Med Biol. 2015; 60:2435–52. [PubMed: 25739661]
134. Ritt S. Design and performance of the 6 GHz waveform digitizing chip DRS4. Nuclear Science Symposium Conference Record, 2008 NSS'08 IEEE. 2008:1512–1515.
135. Ruiz-Gonzalez M, Bora V, Furenlid LR. Maximum-likelihood estimation of scintillation pulse timing. IEEE Trans Rad Plasma Med Sci. 2017
136. Berg E, Cherry SR. Using convolutional neural networks to estimate time-of-flight from PET detector waveforms. Phys Med Biol. 2017 in press.
137. Korpar S, Dolenec R, Križan P, et al. Study of TOF PET using Cherenkov light. Nucl Inst Meth A. 2011; 654:532–538.
138. Yvon D, Renault J-P, Tauzin G, et al. Calipso: An novel detector concept for PET imaging. IEEE Trans Nucl Sci. 2014; 61:60–66.
139. Brunner S, Schaart D. BGO as a hybrid scintillator/Cherenkov radiator for cost-effective time-of-flight PET. Phys Med Biol. 2017; 62:4421–4439. [PubMed: 28358722]
140. Kwon SI, Gola A, Ferri A, et al. Bismuth germanate coupled to near ultraviolet silicon photomultipliers for time-of-flight PET. Phys Med Biol. 2016; 61:L38–47. [PubMed: 27589153]
141. Somlai-Schweiger I, Ziegler S. CHERENCUBE: Concept definition and implementation challenges of a Cherenkov-based detector block for PET. Med Phys. 2015; 42:1825–1835. [PubMed: 25832073]
142. Moriya T, Fukumitsu K, Sakai T, et al. Development of PET detectors using monolithic scintillation crystals processed with sub-surface laser engraving technique. IEEE Trans Nucl Sci. 2010; 57:2455–2459.
143. Uchida H, Sakai T, Yamauchi H, et al. A novel single-ended readout depth-of-interaction PET detector fabricated using sub-surface laser engraving. Phys Med Biol. 2016; 61:6635–50. [PubMed: 27541440]
144. Sabet H, Kudrolli H, Singh B, et al. Fabricating high-resolution and high-sensitivity scintillator arrays using laser induced optical barriers. Nuclear Science Symposium and Medical Imaging Conference (NSS/MIC), 2012 IEEE. 2012:4080–4084.

145. Bläckberg L, El Fakhri G, Sabet H. Simulation study of light transport in laser-processed LYSO: Ce detectors with single-side readout. Phys Med Biol. 2017; 62:8419–8440. [PubMed: 29047453]

146. Yamamoto S, Watabe H, Kanai Y, et al. Development of an ultrahigh resolution Si-PM based PET system for small animals. Phys Med Biol. 2013; 58:7875–88. [PubMed: 24145308]

147. Yang Y, Bec J, Zhang M, et al. A high resolution prototype small-animal PET scanner dedicated to mouse brain imaging. J Nucl Med. 2016; 57:1130–35. [PubMed: 27013696]

148. Stickel JR, Qi J, Cherry SR. Fabrication and characterization of a 0.5-mm lutetium oxyorthosilicate detector array for high-resolution PET applications. J Nucl Med. 2007; 48:115–121. [PubMed: 17204707]

149. Vandenbroucke A, Foudray A, Olcott P, et al. Performance characterization of a new high resolution PET scintillation detector. Phys Med Biol. 2010; 55:5895–911. [PubMed: 20844332]

150. Song TY, Wu H, Komarov S, et al. A sub-millimeter resolution PET detector module using a multi-pixel photon counter array. Phys Med Biol. 2010; 55:2573–87. [PubMed: 20393236]

151. Bergeron M, Cadorette J, Beaudoin J-F, et al. Performance evaluation of the LabPET APD-based digital PET scanner. IEEE Trans Nucl Sci. 2009; 56:10–16.

152. Yamaya T, Mitsuhashi T, Matsumoto T, et al. A SiPM-based isotropic-3D PET detector X'tal cube with a three-dimensional array of 1 mm^3 crystals. Phys Med Biol. 2011; 56:6793–807. [PubMed: 21971079]

153. Llosá G, Barrio J, Lacasta C, et al. Characterization of a PET detector head based on continuous LYSO crystals and monolithic, 64-pixel silicon photomultiplier matrices. Phys Med Biol. 2010; 55:7299–315. [PubMed: 21081823]

154. Seifert S, Van der Lei G, Van Dam HT, et al. First characterization of a digital SiPM based time-of-flight PET detector with 1 mm spatial resolution. Phys Med Biol. 2013; 58:3061–74. [PubMed: 23587636]

155. Marcinkowski R, Mollet P, Van Holen R, et al. Sub-millimetre DOI detector based on monolithic LYSO and digital SiPM for a dedicated small-animal PET system. Phys Med Biol. 2016; 61:2196–2212. [PubMed: 26907952]

156. Borghi G, Tabacchini V, Schaart DR. Towards monolithic scintillator based TOF-PET systems: practical methods for detector calibration and operation. Phys Med Biol. 2016; 61:4904–4928. [PubMed: 27285955]

157. Borghi G, Tabacchini V, Seifert S, et al. Experimental validation of an efficient fan-beam calibration procedure for nearest neighbor position estimation in monolithic scintillator detectors. IEEE Trans Nucl Sci. 2015; 62:57–67.

158. Gu Y, Matteson J, Skelton R, et al. Study of a high-resolution, 3D positioning cadmium zinc telluride detector for PET. Phys Med Biol. 2011; 56:1563–84. [PubMed: 21335649]

159. Mitchell GS, Sinha S, Stickel JR, et al. CdTe strip detector characterization for high resolution small animal PET. IEEE Trans Nucl Sci. 2008; 55:870–876.

160. Ishii K, Kikuchi Y, Matsuyama S, et al. First achievement of less than 1 mm FWHM resolution in practical semiconductor animal PET scanner. Nucl Inst Meth A. 2007; 576:435–440.

161. Groll A, Kim K, Bhatia H, et al. Hybrid pixel-waveform (HPWF) enabled CdTe detectors for small animal gamma-ray imaging applications. IEEE Trans Rad Plasma Med Sci. 2017; 1:3–14.

162. Komarov S, Yin Y, Wu H, et al. Investigation of the limitations of the highly pixelated CdZnTe detector for PET applications. Phys Med Biol. 2012; 57:7355–80. [PubMed: 23079763]

163. Churilov AV, Higgins WM, Ciampi G, et al. Purification, crystal growth and detector performance of TlBr. Proc SPIE. 2008; 70790

164. Hitomi K, Tada T, Onodera T, et al. Timing performance of TlBr detectors. IEEE Trans Nucl Sci. 2013; 60:2883–2887.

165. Arino-Estrada G, Mitchell GS, Kwon SI, et al. Towards time-of-flight PET with a semiconductor detector. Phys Med Biol. 2018 in press.

166. Schmall JP, Karp JS, Werner M, et al. Parallax error in long-axial field-of-view PET scanners—a simulation study. Phys Med Biol. 2016; 61:5443–5455. [PubMed: 27367971]

167. Yang Y, Dokhale PA, Silverman RW, et al. Depth of interaction resolution measurements for a high resolution PET detector using position sensitive avalanche photodiodes. Phys Med Biol. 2006; 51:2131–2142. [PubMed: 16625031]
168. Dokhale P, Silverman R, Shah KS, et al. Performance measurements of a depth-encoding PET detector module based on position-sensitive avalanche photodiode read-out. Phys Med Biol. 2004; 49:4293–304. [PubMed: 15509066]
169. Huber J, Moses W, Andreaco M, et al. A LSO scintillator array for a PET detector module with depth of interaction measurement. Nuclear Science Symposium Conference Record, 2000 IEEE. 2000; 2:14/46–14/50.
170. Maas MC, Schaart DR, van der Laan DJ, et al. Monolithic scintillator PET detectors with intrinsic depth-of-interaction correction. Phys Med Biol. 2009; 54:1893–908. [PubMed: 19265203]
171. Ling T, Lewellen T, Miyaoka R. Depth of interaction decoding of a continuous crystal detector module. Phys Med Biol. 2007; 52:2213–2228. [PubMed: 17404465]
172. Gagnon D, Pouliot N, Laperriere L, et al. Maximum likelihood positioning in the scintillation camera using depth of interaction. IEEE Trans Med Imag. 1993; 12:101–107.
173. Vinke R, van Dam HT, Seifert S, et al. Thick monolithic scintillation crystals for TOF-PET with depth-of-interaction measurement. IEEE Nuclear Science Symposuim & Medical Imaging Conference. 2010:1981–1984.
174. Yamamoto S, Imaizumi M, Watabe T, et al. Development of a Si-PM-based high-resolution PET system for small animals. Phys Med Biol. 2010; 55:5817–31. [PubMed: 20844330]
175. Omura T, Moriya T, Yamada R, et al. Development of a high-resolution four-layer DOI detector using MPPCs for brain PET. Nuclear Science Symposium and Medical Imaging Conference (NSS/MIC), 2012 IEEE. 2012:3560–3563.
176. Thompson CJ, Goertzen AL, Berg EJ, et al. Evaluation of high density pixellated crystal blocks with SiPM readout as candidates for PET/MR detectors in a small animal PET insert. IEEE Trans Nucl Sci. 2012; 59:1791–1797.
177. Liu H, Omura T, Watanabe M, et al. Development of a depth of interaction detector for γ-rays. Nucl Inst Meth A. 2001; 459:182–190.
178. Tsuda T, Furumiya T, Ohi J, et al. Development of a TOF-PET detector capable of four-layer DOI encoding with a single-layer crystal array. Nuclear Science Symposium and Medical Imaging Conference (NSS/MIC), 2011 IEEE. 2011:3012–3014.
179. Liu S, An S, Li H, et al. A dual-layer TOF-DOI detector block for whole-body PET. IEEE Trans Nucl Sci. 2012; 59:1805–1808.
180. Bauer F, Aykac M, Eriksson L, et al. Depth of interaction with a 3-dimensional checkerboard arrangement LSO-LSO block. IEEE Trans Nucl Sci. 2010; 57:971–975.
181. Wiener R, Surti S, Karp JS. DOI determination by rise time discrimination in single-ended readout for TOF PET imaging. IEEE Trans Nucl Sci. 2013; 60:1478–1486. [PubMed: 24403611]
182. Du H, Yang Y, Glodo J, et al. Continuous depth-of-interaction encoding using phosphor-coated scintillators. Phys Med Biol. 2009; 54:1757–1771. [PubMed: 19258685]
183. Berg E, Roncali E, Hutchcroft W, et al. Improving depth, energy and timing estimation in PET detectors with deconvolution and maximum likelihood pulse shape discrimination. IEEE Trans Med Imag. 2016; 35:2436–2446.
184. Berg E, Roncali E, Kapusta M, et al. A combined time-of-flight and depth-of-interaction detector for total-body positron emission tomography. Med Phys. 2016; 43:939–950. [PubMed: 26843254]
185. Kwon SI, Ferri A, Gola A, et al. Reaching 200-ps timing resolution in a time-of-flight and depth-of-interaction positron emission tomography detector using phosphor-coated crystals and high-density silicon photomultipliers. J Med Imaging. 2016; 3:043501.
186. Schmall JP, Roncali E, Berg E, et al. Timing properties of phosphor-coated polished LSO crystals. Phys Med Biol. 2014; 59:N139–51. [PubMed: 25047008]
187. Lecoq P. Development of new scintillators for medical applications. Nucl Inst Meth A. 2016; 809:130–139.
188. Yeom JY, Yamamoto S, Derenzo SE, et al. First performance results of Ce:GAGG scintillation crystals with silicon photomultipliers. IEEE Trans Nucl Sci. 2013; 60:988–992.

189. Wu Y, Luo Z, Jiang H, et al. Single crystal and optical ceramic multicomponent garnet scintillators: A comparative study. Nucl Inst Meth A. 2015; 780:45–50.

190. Shah K, Glodo J, Klugerman M, et al. High energy resolution scintillation spectrometers. IEEE Trans Nucl Sci. 2004; 51:2395–2399.

191. Van Loef E, Dorenbos P, Van Eijk C, et al. Scintillation properties of $LaBr_3$:Ce^{3+} crystals: fast, efficient and high-energy-resolution scintillators. Nucl Inst Meth A. 2002; 486:254–258.

192. Alekhin MS, De Haas J, Khodyuk I, et al. Improvement of γ-ray energy resolution of $LaBr_3$: Ce^{3+} scintillation detectors by Sr^{2+} and Ca^{2+} co-doping. Appl Phys Lett. 2013; 102:161915.

193. Quarati F, Alekhin M, Krämer K, et al. Co-doping of $CeBr_3$ scintillator detectors for energy resolution enhancement. Nucl Inst Meth A. 2014; 735:655–658.

194. Levin CS, Foudray AM, Habte F. Impact of high energy resolution detectors on the performance of a PET system dedicated to breast cancer imaging. Physica Medica. 2006; 21:28–34. [PubMed: 17645990]

195. Kim H, Cirignano L, Churilov A, et al. Developing larger TlBr detectors—detector performance. IEEE Trans Nucl Sci. 2009; 56:819–823.

196. Ariño G, Chmeissani M, De Lorenzo G, et al. Energy and coincidence time resolution measurements of CdTe detectors for PET. J Instr. 2013; 8:C02015.

197. Hitomi K, Kikuchi Y, Shoji T, et al. Improvement of energy resolutions in TlBr detectors. Nucl Inst Meth A. 2009; 607:112–115.

198. Berg E, Zhang X, Bec J, et al. Development and evaluation of mini-EXPLORER: a long axial field-of-view PET scanner for non-human primate imaging. J Nucl Med. 2018 in press.

199. Taguchi K, Iwanczyk JS. Vision 20/20: Single photon counting x-ray detectors in medical imaging. Med Phys. 2013; 40:100901. [PubMed: 24089889]

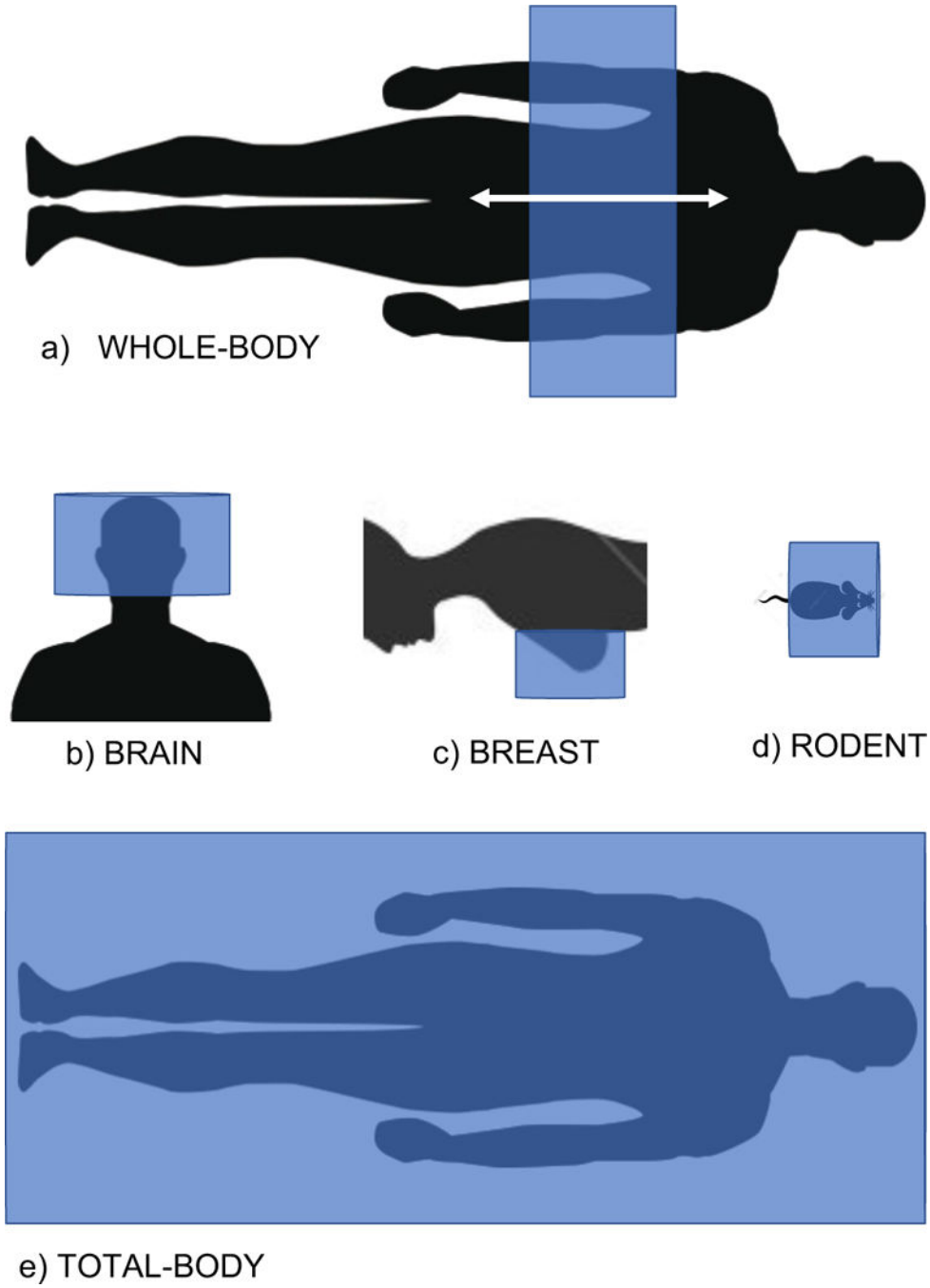

Figure 1.

Illustration of relative geometry of a) standard whole-body clinical PET scanner where the patient is translated through the scanner to create a whole-body image from multiple bed positions; b) dedicated brain PET scanner; c) dedicated breast PET scanner with patient lying in prone position; d) preclinical PET scanner for rodent imaging; and e) extended field of view scanner for total-body PET imaging. The physical extent of the PET scanners are indicated in blue and typically consist of rings of detectors around the subject or organ.

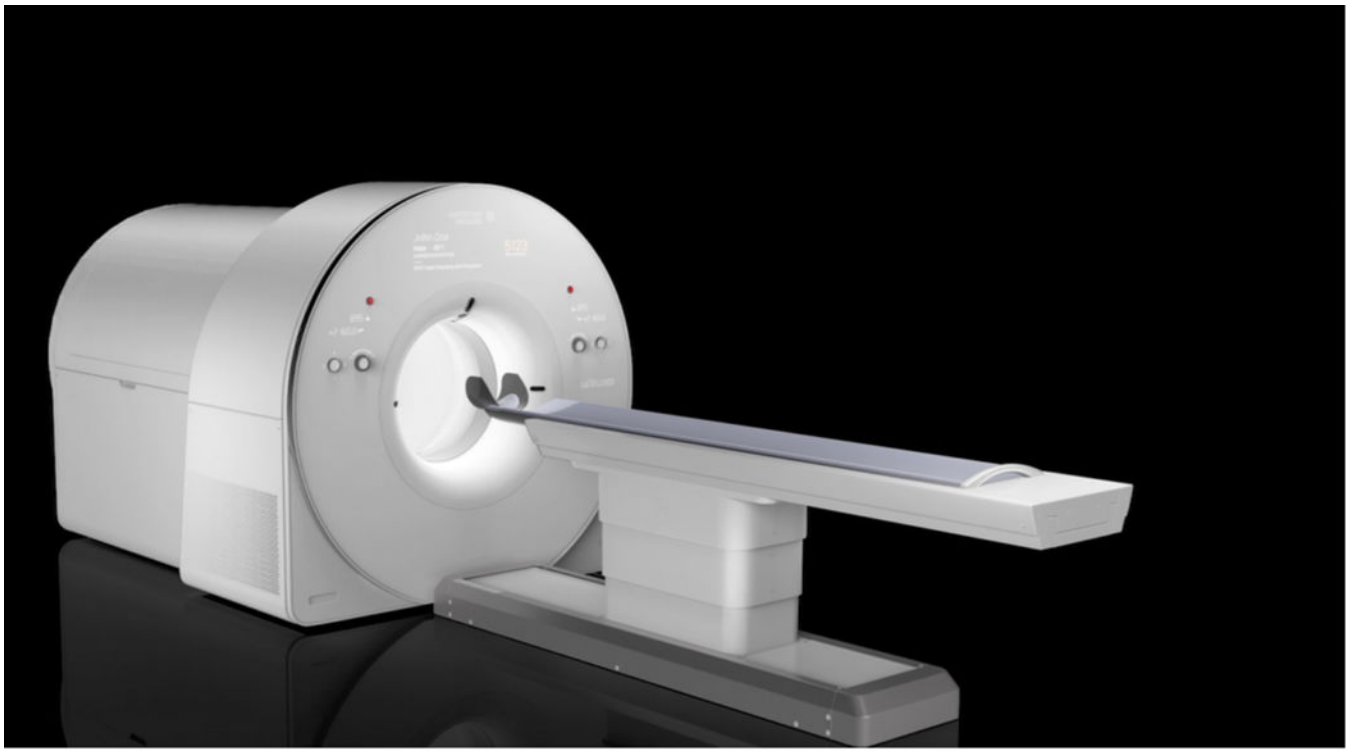

Figure 2.
Photograph of the EXPLORER total-body PET scanner which is currently under construction (courtesy United Imaging Healthcare, Shanghai, China).

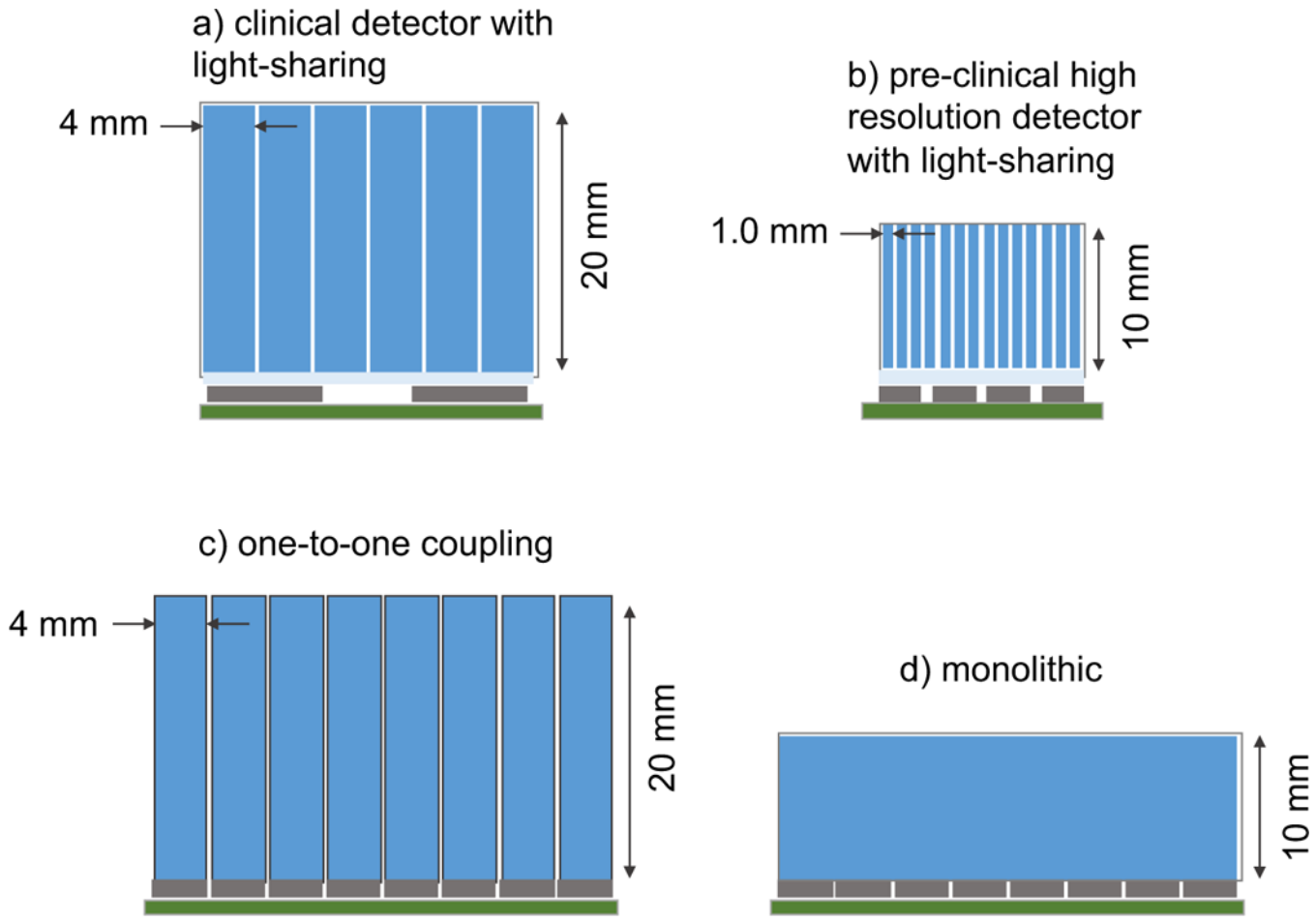

Figure 3.

Illustration of different detector designs used in PET. a) Light sharing clinical block detector, b) high resolution light sharing pre-clinical detector, c) one-to-one coupled detector, and d) monolithic detector. Dark blue represents the scintillator crystals, light blue represents the light guide, brown represents the photodetectors (i.e. SiPMs), and green represents the electronic circuits. Crystal dimensions represent common detector designs.

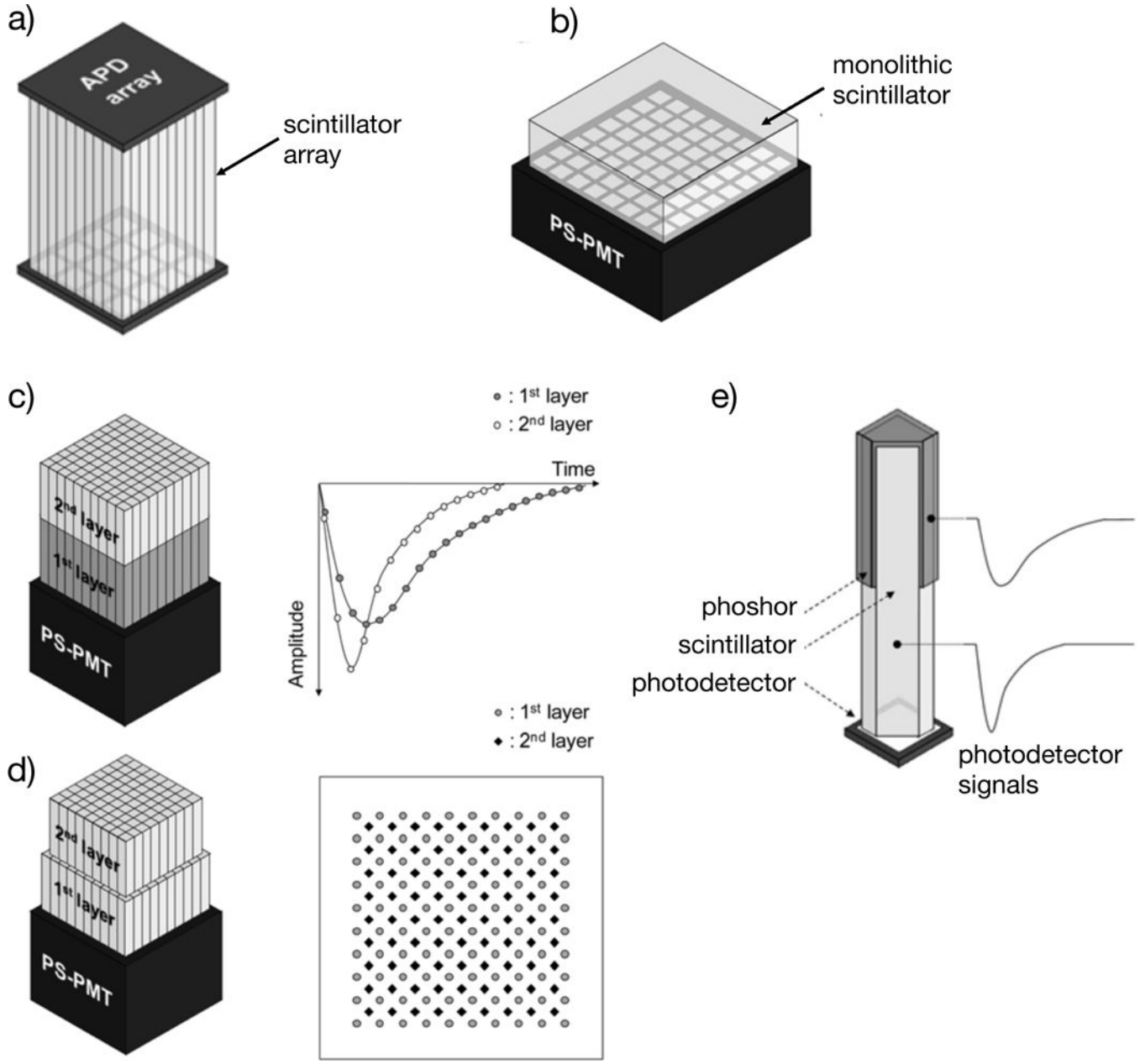

Figure 4.

Overview of common DOI encoding methods for PET detectors. a) Dual-ended readout, where photodetectors (i.e. APDs or SiPMs) are fastened to both ends of a pixelated scintillator array to measure DOI-dependent differences in light collection. b) monolithic detectors, where an array of photodetectors measures DOI-dependent differences in the spread of scintillation light. c) the phoswich detector which uses two or more layers of scintillators that vary in their scintillation emission properties (e.g. decay time). d) a stacked scintillator configuration where the top scintillator array is offset by ½ crystal pitch so that the distribution of light from the top layer is unique from the bottom layer as measured by a set of photodetectors. e) phosphor-coated detector, where a thin layer of phosphor coating

applied to the sides of the scintillator crystal induces DOI-dependent signal shape changes. Reproduced with permission from [38].